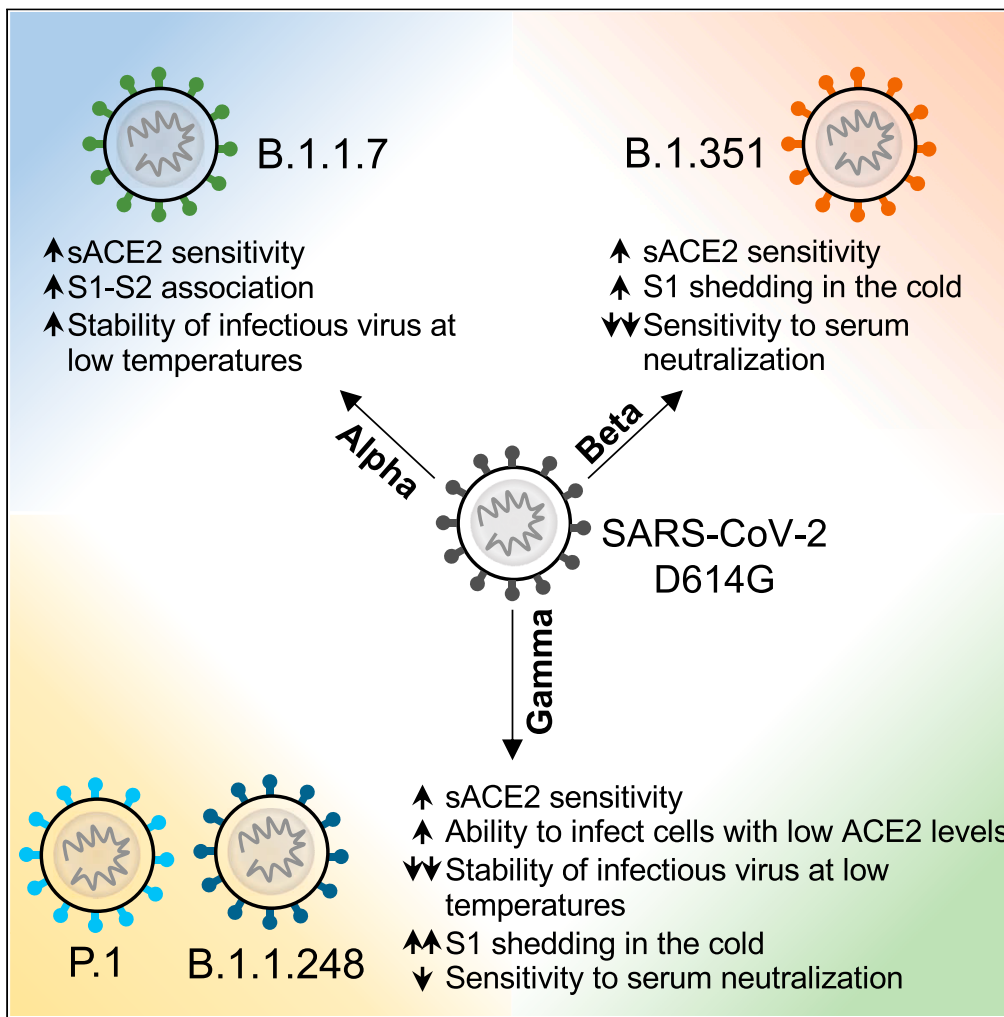**Article**

Functional differences among the spike glycoproteins of multiple emerging severe acute respiratory syndrome coronavirus 2 variants of concern

Qian Wang, Manoj
S. Nair, Saumya
Anang, ..., Lihong
Liu, David D. Ho,
Joseph G.
Sodroski

joseph_sodroski@dfci.harvard.
edu

Highlights

Spikes of emerging SARS-
CoV-2 variants exhibit
increased affinity for ACE2
receptor

P.1 and B.1.1.248 exhibit
increased ability to infect
cells with low ACE2 levels

More stable functional
B.1.1.7 spike and less
stable P.1/B.1.1.248
spikes in cold

B.1.351/P.1/B.1.1.248 are
neutralized less well by
convalescent and
vaccinee sera

Article

Functional differences among the spike glycoproteins of multiple emerging severe acute respiratory syndrome coronavirus 2 variants of concern

Qian Wang,[1,4] Manoj S. Nair,[2,4] Saumya Anang,[1] Shijian Zhang,[1] Hanh Nguyen,[1] Yaoxing Huang,[2] Lihong Liu,[2] David D. Ho,[2] and Joseph G. Sodroski[1,3,5,*]

SUMMARY

We compared the functional properties of spike (S) glycoproteins from the original SARS-CoV-2 strain (D614) (Wuhan, China), the globally dominant D614G strain, and emerging geographic variants: B.1.1.7 (United Kingdom), B.1.351 (South Africa), P.1 (Brazil), and B.1.1.248 (Brazil/Japan). Compared with D614G, the emerging variants exhibited an increased affinity for the receptor, ACE2, and increased ability to infect cells with low ACE2 levels. All variants lost infectivity similarly at room temperature and 37°C; however, in the cold, B.1.1.7 was more stable, and P.1 and B.1.1.248 were less stable. Shedding of the S1 glycoprotein from the S contributed to virus inactivation in the cold. B.1.351, P.1, and B.1.1.248 were neutralized by convalescent and vaccinee sera less efficiently than the other variants. S glycoprotein properties such as requirements for ACE2 levels on the target cell, functional stability in the cold, and resistance to host neutralizing antibodies potentially contribute to the outgrowth of emerging SARS-CoV-2 variants.

INTRODUCTION

The COVID-19 pandemic caused by the SARS-CoV-2 coronavirus has severely impacted global health, world economy, and quality of life (Hu et al., 2021; Nicola et al., 2020; Wang et al., 2020). Over the past several months, intensive efforts have been placed on vaccine production and distribution, raising hope for the possibility of curtailing and controlling the virus' spread (Krammer, 2020; Ng et al., 2020). Multiple vaccine approaches employing SARS-CoV-2 spike (S) glycoprotein immunogens have demonstrated significant clinical efficacy (Anderson et al., 2020; AstraZeneca, 2021; Baden et al., 2021; Johnson, 2021; Novavax, 2021; Polack et al., 2020; Voysey et al., 2021; Xia et al., 2021). Although the results are promising, the virus has continued to evolve; as early as November 2020, the first reports of global variants with higher transmissibility rates were released (du Plessis et al., 2021; Kupferschmidt, 2021). Changes in the genome resulting from the replication of RNA viruses such as SARS-CoV-2 are not unexpected, but indications that these new strains of SARS-CoV-2 exhibit increased transmissibility, pathogenicity, and/or susceptibility to neutralizing antibodies are concerning (Davies et al., 2021a, 2021b; Tegally et al., 2020). Consequently, the Centers for Disease Control and Prevention has designated several newly emergent strains (B.1.1.7, B.1.351, P.1, and B.1.427) as "variants of concern" (CDC, 2021).

Shortly after the beginning of the COVID-19 pandemic, a SARS-CoV-2 strain with a D614G alteration in the S glycoprotein arose that exhibited greater S stability and infectivity than the original virus from Wuhan, China (Korber et al., 2020; Li et al., 2020; Zhang et al., 2020, 2021). The D614G variant quickly became globally dominant (Korber et al., 2020). Additional SARS-CoV-2 variants have emerged as descendants of this D614G strain, including B.1.1.7 (identified in the United Kingdom), B.1.351 (identified in South Africa), P.1 (prevalent in Brazil), and B.1.1.248 (identified in travelers to Japan from Brazil) (Fujino et al., 2021; Kupferschmidt, 2021; National Institute of Infectious Diseases, 2021; Tegally et al., 2020). Studies have demonstrated that the observed changes in the S glycoproteins of these variants decrease the sensitivity of the virus to neutralization by monoclonal antibodies or vaccine-induced antisera (Hoffmann et al., 2021; Wang et al., 2021a, 2021b, 2021c). Clinical trials of some vaccines have suggested a reduction in efficacy against the B.1.351 variant (Voysey et al., 2021; Wang et al., 2021d; Wu et al., 2021).

[1]Department of Cancer Immunology and Virology, Dana-Farber Cancer Institute, Department of Microbiology, Harvard Medical School, Boston, MA 02215, USA

[2]Aaron Diamond AIDS Research Center, Columbia University Vagelos College of Physicians and Surgeons, New York, NY 10032, USA

[3]Department of Immunology and Infectious Diseases, Harvard T.H. Chan School of Public Health, Boston, MA 02215, USA

[4]These authors contributed equally

[5]Lead contact

*Correspondence: joseph_sodroski@dfci.harvard.edu

https://doi.org/10.1016/j.isci.2021.103393

Although each of the emerging SARS-CoV-2 variants exhibits changes throughout their proteome, such changes particularly cluster in the S glycoprotein, the viral surface protein that mediates virus entry and thus represents the predominant target of antibodies. The coronavirus S is a glycosylated trimer composed of two subunits, S1 and S2 (Bosch et al., 2003). The receptor-binding S1 subunit is relatively exposed, whereas much of S2 is buried as a transmembrane subunit. As such, neutralizing antibody responses are primarily directed against the S1 subunit (Isho et al., 2020). The S1 subunit is further subdivided into an N-terminal domain (NTD) and receptor-binding domain (RBD), both of which are targets of neutralizing antibodies (Liu et al., 2020).

Several studies have examined the impact of S variation in emerging SARS-CoV-2 strains on virus susceptibility to host antibody responses (Hoffmann et al., 2021; Wang et al., 2021a, 2021b, 2021c), but fewer studies have examined the functional properties of the mutant S glycoproteins. The multitude of changes in the S glycoproteins that become fixed in these variants supports their potential importance to transmission, pathogenesis, and/or immune evasion. Indeed, some of the observed changes enhance S glycoprotein binding to the receptor, angiotensin-converting enzyme 2 (ACE2) (Gobeil et al., 2021; Laffeber et al., 2021).

Here, we examine the functional properties of the S glycoproteins of the emerging SARS-CoV-2 variants B.1.1.7, B.1.351, P.1, and B.1.1.248. Using vesicular stomatitis virus (VSV) and human immunodeficiency virus (HIV-1) pseudotypes, we evaluated the expression, post-translational processing, infectivity, stability at various temperatures, and sensitivity to neutralization of the variants. The overall level of expression, processing. and glycosylation of the variant S glycoproteins in cell lysates and pseudovirus particles were similar to those of the original (D614) SARS-CoV-2 strain from Wuhan, China. Notably, compared with the D614 S glycoprotein, the S glycoproteins of the emerging variants required less ACE2 receptor expression on the target cell to mediate virus entry. This enhanced infection efficiency was in part explained by a 2- to 9-fold increase in ACE2 binding affinity. Although the infectivity of the S glycoprotein-pseudotyped viruses decayed comparably at room temperature (RT) and 37°C, marked differences in susceptibility to cold inactivation, which reflects the stability of the trimeric S, were observed. At 0°C, P.1 and B.1.1.248 spontaneously shed the S1 glycoprotein from the trimer and lost infectivity, whereas B.1.1.7 exhibited greater S stability and was more resistant to cold inactivation than D614. The authentic B.1.1.7 SARS-CoV-2 variant resisted cold inactivation more than the other viruses tested. Soluble ACE2 (sACE2) binding at 37°C resulted in the shedding of the S1 glycoprotein from the trimer of all strains tested; however, strain-dependent differences in sACE2-induced shedding were observed at 0°C. Finally, the B.1.351, P.1, and B.1.1.248 pseudoviruses were more resistant to neutralization by sera from convalescent American COVID-19 patients than the other variants tested. The B.1.351 variant, in the context of pseudovirus and authentic SARS-CoV-2, was less sensitive to neutralization by sera from recipients of the Moderna COVID-19 vaccine. These unique properties of the S glycoproteins potentially influence the transmissibility, prevention. and pathogenesis of the emerging SARS-CoV-2 variants.

RESULTS

S glycoprotein processing, subunit association, and incorporation into virus particles

In this study, we compare the functional phenotypes of the S glycoproteins of the newly emergent SARS-CoV-2 variants B.1.1.7, B.1.351, P.1, and B.1.1.248 with those of the early/founder virus (D614) and the globally prevalent D614G variant (Korber et al., 2020; Volz et al., 2021). Figure 1A shows the amino acid substitutions found in the emerging S glycoproteins relative to the D614 strain. The more recently emerged B.1.1.7, B.1.351, P.1, and B.1.1.248 variants are the offspring of the D614G strain and therefore all contain the D614G change. The B.1.1.7 variant, first identified in Southeast England in September 2020 and now the dominant strain in the United Kingdom (Kupferschmidt, 2021), has 8 additional S glycoprotein changes, including 2 deletions in the NTD and an N501Y change in the RBD. The B.1.351 variant emerged in South Africa in October 2020 (Tegally et al., 2020) and has 9 S glycoprotein changes in addition to D614G, including three in the RBD and several in the NTD. The P.1 variant is prevalent in Brazil; in addition to D614G, P.1 has 10 changes, three of which are similar to those in the RBD of B.1.351 (Fujino et al., 2021). P.1 also has five changes in the NTD, two of which introduce new potential N-linked glycosylation sites. Compared with the P.1 variant, the B.1.1.248 variant, which was identified in travelers to Japan from Brazil, has one change in HR2 (National Institute of Infectious Diseases, 2021).
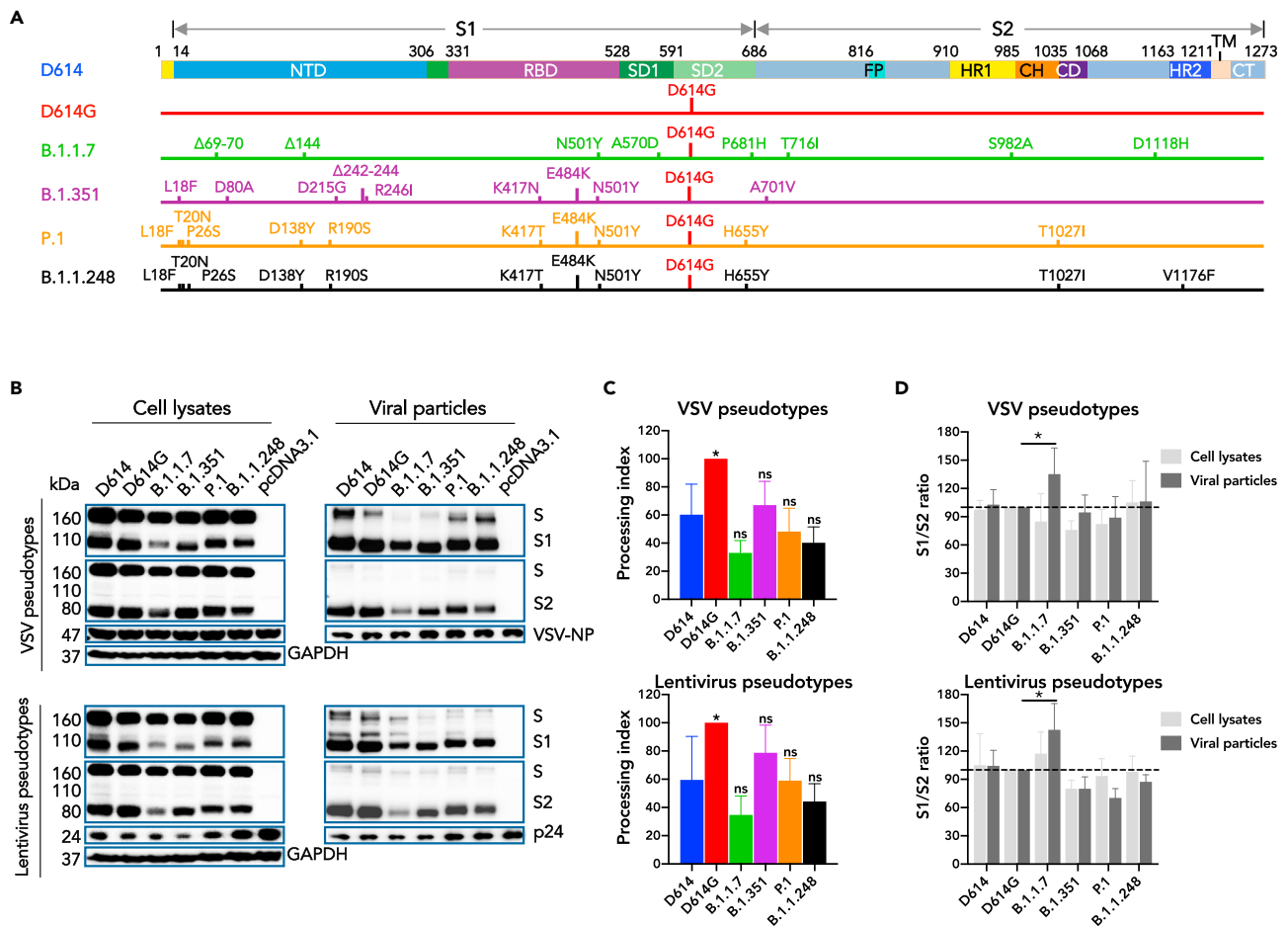
Figure 1. Processing, subunit association, and incorporation into virus particles of SARS-CoV-2 variant S glycoproteins

(A) A schematic representation is shown in the upper figure of the wild-type (D614) S glycoprotein from the SARS-CoV-2 strain responsible for the initial outbreak in Wuhan, Hubei province, China. The NTD, RBD, and subdomains 1 and 2 (SD1 and SD2) of the S1 glycoprotein are indicated. The fusion peptide (FP), heptad repeat regions (HR1 and HR2), central helical region (CH), connector domain (CD), transmembrane region (TM), and cytoplasmic tail (CT) of the S2 glycoprotein are indicated. The amino acid changes in the indicated SARS-CoV-2 natural variants are shown in the diagrams beneath the schematic.

(B) HEK293T cells producing VSV (upper panels) and lentiviral (lower panels) particles pseudotyped with the indicated SARS-CoV-2 S glycoproteins were used to prepare cell lysates (left panels) and viral particles (right panels), which were Western blotted with rabbit anti-S1 and anti-S2 antibodies. The samples were also Western blotted with anti-VSV NP (upper panels), anti-HIV p17/p24/p55 (lower panels), and anti-GAPDH antibodies. The Western blots shown are representative of those obtained in four independent experiments. Cells transfected with the pcDNA3.1 vector were used as a negative control.

(C) Processing indices were calculated from Western blots of cell lysates from multiple experiments, as described (Nguyen et al., 2020). The processing index of each S glycoprotein variant was compared with that of D614 using a Student's unpaired t test (*p < 0.05; ns – not significant). Data are represented as mean ± SEM.

(D) The intensities of the S1 and S2 glycoprotein bands in Western blots derived from four independent experiments described in (B) were measured. The average S1/S2 ratio was calculated and compared with that of D614G. Statistical analysis was performed using a Student's unpaired t test (*p < 0.05). Data are represented as mean ± SEM.

We studied the expression, processing, subunit association, and incorporation into pseudotyped virus particles of the variant SARS-CoV-2 S glycoproteins. We generated VSV and lentivirus (HIV-1) particles as previously described (Schmidt et al., 2020). The D614 and variant S glycoproteins were expressed in 293T cells followed by VSVΔG infection or were expressed in combination with lentiviral vector constructs. Subsequently, the S glycoproteins in the cell lysates and on the VSV/lentiviral particles were examined by Western blot. The uncleaved S precursor, as well as the cleaved S1 and S2 proteins, were evident in the cell lysates and on VSV/lentiviral particles (Figure 1B). The majority of the S glycoproteins incorporated into VSV/lentiviral particles were cleaved into S1 and S2, whereas a higher ratio of uncleaved S precursor was present in the cell lysates. Most of the variant S glycoproteins were processed and incorporated into viral particles comparably; the proteolytic processing of D614G was slightly more efficient than that of D614 (Figure 1C),

as has been previously seen (Nguyen et al., 2020). The S1/S2 ratio on VSV and lentiviral particles was higher for B.1.1.7 than that of the D614 and other variants (Figure 1D), suggesting a tighter association of the B.1.1.7 S1 glycoprotein with the viral S.

Glycosylation of the severe acute respiratory syndrome coronavirus 2 S glycoprotein variants

To study the glycosylation of the SARS-CoV-2 D614 and variant S glycoproteins, cell lysates and VSV/lentiviral particles from S-expressing 293T cells were treated with PNGase F and Endo Hf. PNGase F removes almost all types of N-linked glycosylation, including high-mannose, hybrid, bi-, tri-, and tetra-antennary glycans, whereas Endo Hf selectively removes high-mannose and some hybrid types of N-linked carbohydrates. The glycosylation patterns of S glycoproteins on pseudotyped VSV particles (Figure 2A) and lentiviral particles (Figure 2B) were similar. S glycoprotein precursors in 293T cell lysates were mainly modified by high-mannose glycans. In contrast, the cleaved S1 and S2 glycoproteins contained mostly complex carbohydrates. The ratio of cleaved:uncleaved S glycoproteins in viral particles was increased compared with that in cell lysates. Multiple S1 and S2 bands from the cell lysate samples treated with glycosidases were detected, indicating diverse post-translational modification of the S1 and S2 subunits. Following PNGase F digestion, the S2 glycoproteins incorporated into virus particles were more homogeneous than those in cell lysates.

The untreated and the Endo Hf-treated S1 from P.1 and B.1.1.248 migrated slightly slower than that of D614G. The two additional potential N-linked glycosylation sites created by the T20N and R190S changes in the NTDs of P.1 and B.1.1.248 S1 glycoproteins likely account for the observed higher molecular weight. B.1.1.7 S1, which has a deletion of three amino acids relative to D614G, as well as the S2 glycoprotein of P.1 and B.1.1.248, also migrated slower after Endo Hf but not PNGase F treatment, highlighting their additional modification by complex carbohydrates compared with that of D614G.

Analysis of authentic SARS-CoV-2 particles confirmed that the vast majority of the S, S1, and S2 glycoproteins incorporated into virions are modified by complex carbohydrates for all strains examined (Figure 2C).

Cell-cell fusion and virus infection mediated by the S glycoproteins of emerging SARS-CoV-2 variants

We examined the efficiency of cell-cell fusion mediated by the D614 and variant S glycoproteins. We used two platforms to study this function, an alpha-complementation assay and a Tat-based assay. In the former assay, COS-1 effector cells transiently expressing α-gal and the S glycoprotein were co-cultured for 10 h with 293T target cells transiently expressing ω-gal and human ACE2, allowing quantitation of cell-cell fusion by measurement of β-galactosidase activity (Nguyen et al., 2020). In the latter assay, 293T cells expressing Tat and the S glycoprotein were used as donor cells, while TZM-bl cells stably expressing human ACE2 (TZM-bl-ACE2) were used as recipient cells. Cell-cell fusion of the cocultured donor and recipient cells results in the activation of luciferase by HIV-1 Tat. In both systems, the SARS-CoV-2 S glycoprotein variants mediated nearly equivalent levels of cell-cell fusion (Figure 3A). The relative cell-cell fusion activities of the S glycoprotein variants were not changed by varying target cell ACE2 levels (Figure S1) or by coculturing the donor and recipient cells for longer periods of time (data not shown).

To investigate the ability of the variant SARS-CoV-2 S glycoproteins to mediate virus entry, we conducted a single-round infection of target cells by S-pseudotyped VSV and lentiviral particles, as previously described (Schmidt et al., 2020). Infection by VSV pseudotypes was measured on Vero-E6 and 293T-ACE2 cells (Figure 3B), and infection by lentivirus pseudotypes was measured only on 293T-ACE2 cells, as HIV-1 cannot infect Vero-E6 cells. Consistent with previous reports (Korber et al., 2020; Li et al., 2020; Nguyen et al., 2020; Zhang et al., 2020, 2021), D614G exhibited increased infectivity for both Vero-E6 and 293T-ACE2 cells compared with that of D614 (Figure 3B). The P.1 and B.1.1.248 variants exhibited ~4-fold higher infectivity for Vero-E6 cells relative to that of D614G; the B.1.1.7 and B.1.351 variants entered these cells with an efficiency similar to that of D614G. Of note, the difference in infectivity between the P.1 and B.1.1.248 variants and the other variants was less prominent on 293T-ACE2 target cells, irrespective of the pseudovirus backbone. Overall, our data indicate that the P.1 and B.1.1.248 S glycoprotein variants support a higher level of infectivity than that of D614, to a degree dependent on the target cell.

One explanation for the observed target cell dependency of S-glycoprotein-mediated infection in Figure 3B is variation in the level of the ACE2 receptor on the target cell. To test this hypothesis, we
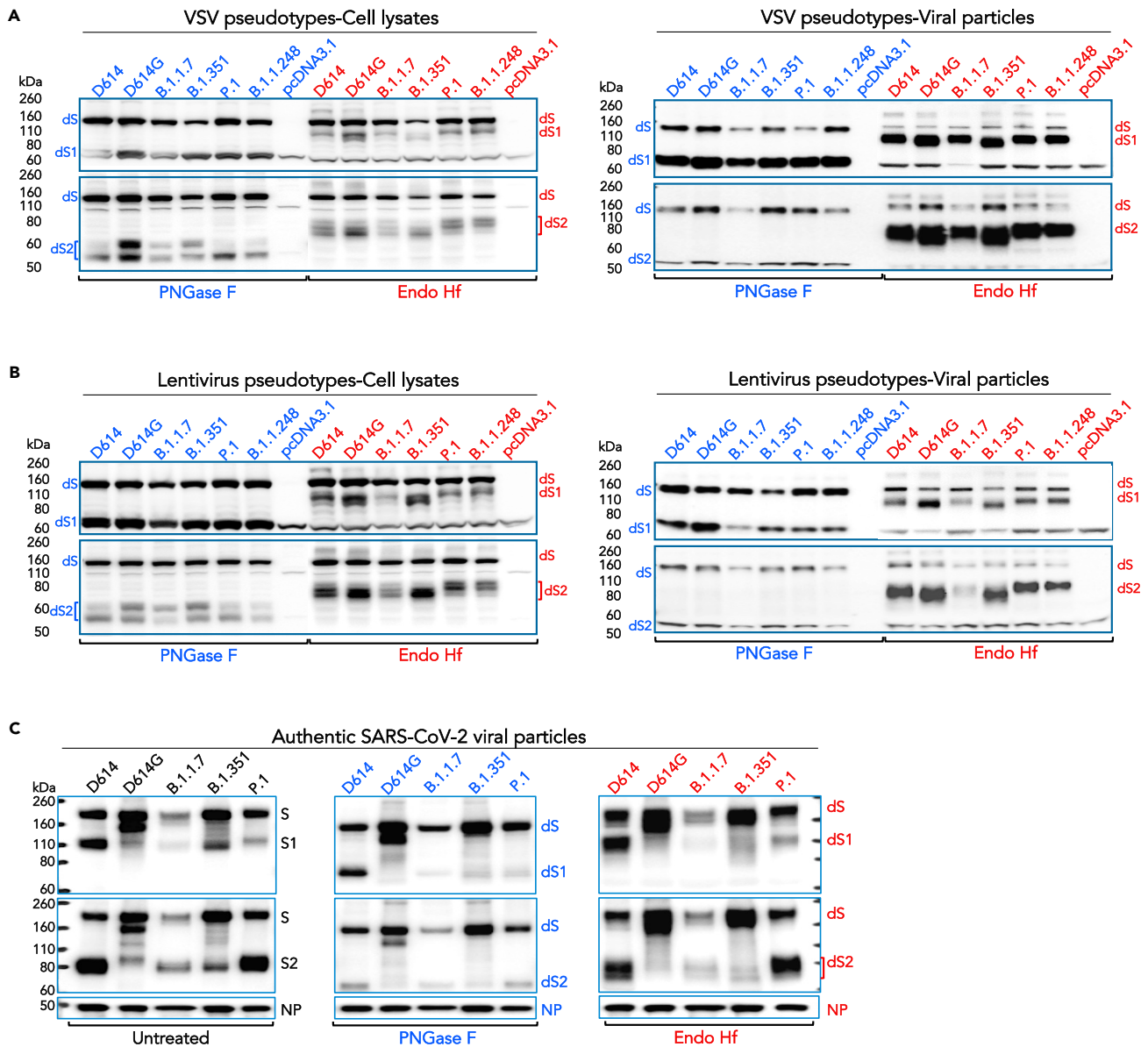
Figure 2. Glycosylation of the S glycoproteins of SARS-CoV-2 variants

(A–C) HEK293T cells producing VSV (A) and lentiviral (B) particles pseudotyped with the indicated SARS-CoV-2 S glycoproteins were used to prepare cell lysates (left panels) and viral particles (right panels). The cell lysates and viral particle preparations were treated with PNGase F and Endo Hf, and the deglycosylated samples were Western blotted with rabbit anti-S1 and anti-S2 antibodies. Cells transfected with the pcDNA3.1 vector were used as a negative control. In (C), authentic virus particles from the indicated SARS-CoV-2 strains were prepared from the supernatants of infected Vero-E6 cells. Virion lysates were treated with PNGase F or Endo Hf and analyzed as described above. The deglycosylated forms of the S glycoprotein precursor (dS), S1 subunit (dS1), and S2 subunit (dS2) are indicated. NP, nucleocapsid (N) protein. The Western blots shown are representative of those obtained in two independent experiments.

transfected 293T cells with different doses of an ACE2-expressing plasmid and then evaluated the infectivity of VSV pseudotypes on these target cells. We confirmed that ACE2 expression on the surface of the transfected 293T cells was dependent on plasmid dose (Figures 3C and 3D). The level of ACE2 influenced the relative infectivity of the VSV vectors pseudotyped by the variant SARS-CoV-2 glycoproteins (Figure 3E). The 293T cells express a low level of endogenous ACE2, allowing some infection by the S-pseudotyped viruses (Figure 3E, left panel). At low ACE2 expression levels, the relative infectivity of the variants exhibited the rank order: P.1, B.1.1.248 > B.1.351 > B.1.1.7 > D614G > D614. At higher ACE2 expression levels, the infectivity of all the viruses increased and the relative differences in infectivity
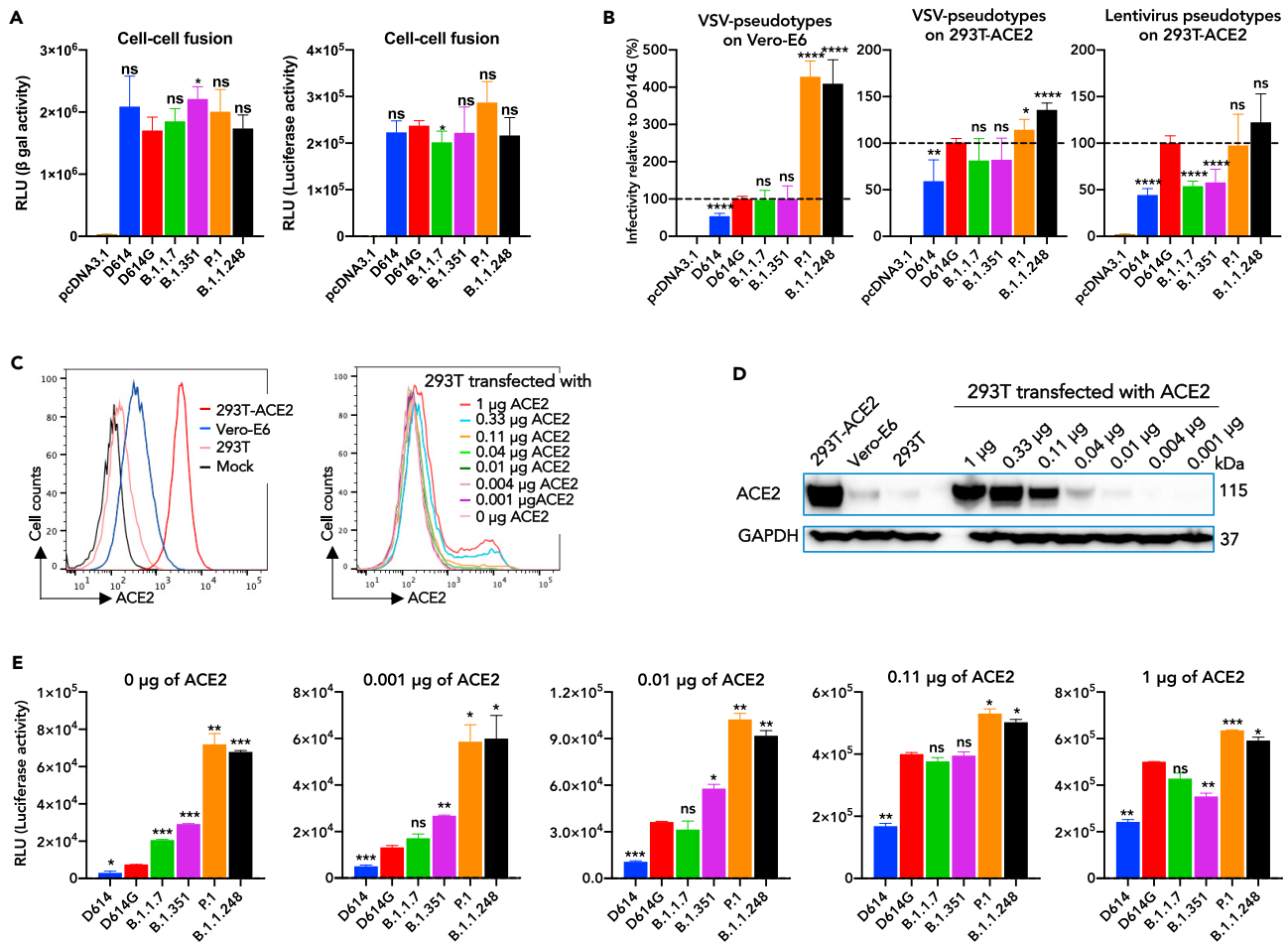
Figure 3. Cell-cell fusion and virus infection mediated by the S glycoproteins of SARS-CoV-2 variants

(A) Cell-cell fusion efficiency between COS-1 effector cells transiently expressing α-gal and the indicated S glycoprotein and 293T target cells transiently expressing ω-gal and human ACE2 was determined by quantitation of β-galactosidase activity in fused cells (left panel). Cell-cell fusion efficiency between donor 293T cells co-transfected with HIV-1 Tat and variant S glycoproteins and target TZM-bl cells stably expressing human ACE2 was determined by quantitation of luciferase activity in fused cells (right panel). The cell-cell fusion activity of each SARS-CoV-2 variant S glycoprotein was compared with that of D614G. In both assays, cells transfected with pcDNA3.1 serve as negative controls. The results shown represent the means and standard deviations derived from three independent experiments. See also Figure S1.

(B) The infectivity of VSV vectors pseudotyped by the indicated SARS-CoV-2 S glycoproteins was determined on Vero-E6 cells (left panel) and 293T-ACE2 cells (middle panel). The infectivity of lentiviral vectors pseudotyped with the variant S glycoproteins was measured on 293T-ACE2 cells (right panel). The measured infectivity was normalized to that observed for the D614G variant. The pcDNA3.1-transfected cells serve as a negative control. The results shown represent the means and standard deviations derived from three independent experiments.

(C) FACS analysis of ACE2 expression on 293T, 293T-ACE2, and Vero-E6 cells is shown in the left panel. FACS analysis of ACE2 expression on 293T cells transfected with the indicated amounts of an ACE2-expressing plasmid is shown in the right panel. Mock represents unstained cells.

(D) Cells from (C) were lysed, and cell lysates were Western blotted for ACE2 or a GAPDH control.

(E) The infectivity of VSV vectors pseudotyped by the variant SARS-CoV-2 S glycoproteins was measured on 293T cells transfected with the indicated amounts of an ACE2-expressing plasmid. The infectivity of each of the pseudoviruses was compared with that of the D614G variant. Note the differences in the scales of the y axes. The means and standard deviations derived from two independent experiments are shown.

Statistical significance in A, B and E was evaluated with a Student's unpaired *t* test (*p < 0.05; **p < 0.01; ***p < 0.001; ****p < 0.0001; ns – not significant).

among the strains diminished. Nonetheless, D614G infected the cells expressing higher ACE2 levels better than D614, and P.1 and B.1.1.248 exhibited slightly higher infectivity than the other variants. The large relative increase in infectivity of P.1 and B.1.1.248 pseudotypes in Vero-E6 cells compared with that in 293T-ACE2 cells could be explained by the lower level of ACE2 expression in these cells (Figure 3C). In summary, compared with the D614 S glycoprotein, the S glycoproteins of the emerging SARS-CoV-2 variants, particularly the P.1 and B.1.1.248 variants, support higher relative infectivity on target cells that express low levels of ACE2.
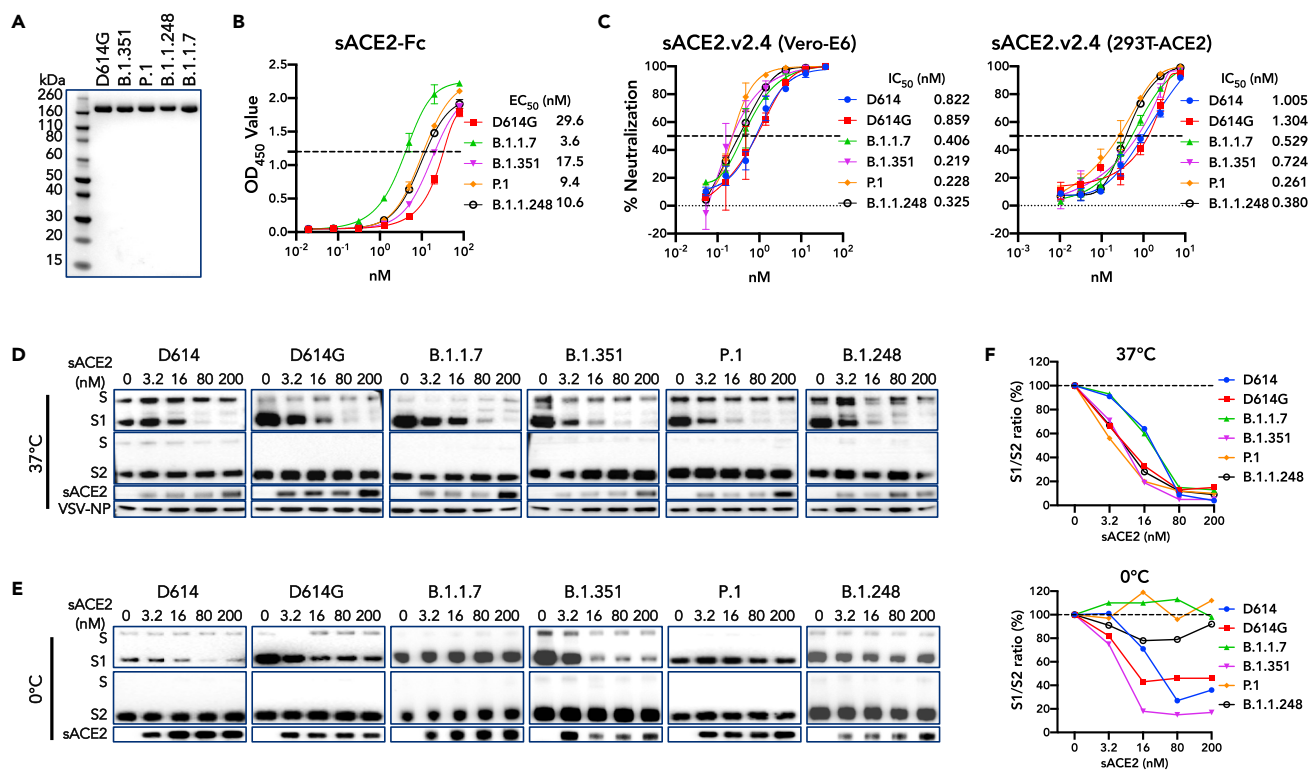
Figure 4. Interaction of soluble ACE2 with the S glycoproteins of SARS-CoV-2 variants

(A) Purified S2P trimers corresponding to the indicated SARS-CoV-2 variant S glycoproteins were analyzed on an SDS-polyacrylamide gel, which was stained with Coomassie Blue.

(B) The S2P trimers in (A) were captured on ELISA plates. Increasing concentrations of soluble ACE2-Fc (sACE2-Fc) protein were incubated with the plates and the bound sACE2-Fc protein was measured. The data in the graph are the means +/− SEM from triplicate measurements obtained in a representative experiment. The concentrations (EC_{50} values) of sACE2-Fc protein required to achieve 50% saturation of binding were calculated and are presented to the right of the graph.

(C) VSV vectors pseudotyped with the indicated S glycoproteins were incubated with increasing concentrations of soluble ACE2.v2.4 (sACE2.v2.4) and then used to infect Vero-E6 cells (left panel) and 293T-ACE2 cells (right panel). The levels of infection were used to determine the % neutralization as a function of sACE2.v2.4 concentration. The results shown in the graphs are the means +/− SEM from triplicate measurements and are representative of those obtained in two independent experiments. The sACE2.v2.4 concentrations resulting in 50% inhibition of infectivity were calculated and are presented to the right of the graphs.

(D and E) VSV particles pseudotyped with the variant SARS-CoV-2 S glycoproteins were incubated with the indicated concentrations of soluble ACE2 (sACE2) for one hour at 37°C (D) and on ice (E). Pelleted VSV particles were analyzed by Western blotting with antibodies against S1, S2, ACE2, and VSV NP.

(F) The intensities of the S1 and S2 glycoprotein bands in (D) and (E) were measured and the S1/S2 ratios for each concentration of sACE2 are shown.

ACE2 binding and sACE2-induced S1 shedding of variant Ss

The above results suggest that changes in the S glycoproteins of emerging SARS-CoV-2 variants may affect their interaction with ACE2. We, therefore, evaluated the binding of soluble S glycoprotein trimers corresponding to D614G and four variants to the sACE2-Fc protein by ELISA (Figures 4A and 4B). The sACE2-Fc protein is a soluble form of the ACE2 receptor fused to the immunoglobulin Fc. All four variants exhibited modest (1.7–8.2-fold) increases in the estimated binding affinity for sACE2-Fc, relative to that of D614G.

We also compared the neutralizing activity of a dimeric soluble ACE2 (sACE2.v2.4) (Chan et al., 2020) against B.1.1.7, B.1.351, P.1, and B.1.1.248 pseudotypes with that against the D614 and D614G pseudotypes. The VSV pseudotypes with D614 and D614G exhibited similar sensitivities to sACE2.v2.4 on Vero-E6 cells (Figure 4C, left) and 293T-ACE2 target cells (Figure 4C, right). The viruses pseudotyped with the four variant S glycoproteins were more sensitive to sACE2.v2.4 on both Vero-E6 cells (2.1- to 3.8-fold) and 293T-ACE2 cells (1.8- to 5.0-fold). The increased sensitivity to sACE2.v2.4 is consistent with greater ACE2 binding and/or responsiveness of the functional B.1.1.7, B.1.351, P.1, and B.1.1.248 variants.

The noncovalent association of S1 and S2 allows spontaneous or soluble ACE2-induced shedding of S1 from the S trimer on SARS-CoV-2 virions, leading to the functional inactivation of the viral S proteins (Nguyen et al., 2020; Zhang et al., 2020). To examine potential differences in S1 shedding from SARS-CoV-2 S glycoprotein variants, we incubated S-pseudotyped VSV particles with various concentrations of soluble ACE2 (sACE2) for one hour at 37°C and on ice. Viruses were then pelleted, washed, and lysed, after which the viral lysates were Western blotted with antibodies against S1, S2, and ACE2 (Figures 4D and 4E). We quantified the blots and examined the S1/S2 ratio (Figure 4F) as an indicator of the S1/S2 association. At 37°C, sACE2 induced S1 shedding from all the VSV pseudotypes, with D614G, B.1.351, P.1, and B.1.1.248 shedding S1 slightly more efficiently than D614 and B.1.1.7. Interestingly, the pattern of sACE2-induced S1 shedding differed on ice, with D614, D614G, and B.1.351 exhibiting more efficient S1 shedding than B.1.1.7, P.1, and B.1.1.248. Thus, while the responses of the variant S glycoproteins to sACE2 differed only modestly at 37°C, significant differences in this property were revealed at a colder temperature.

Stability of variant SARS-CoV-2 Ss at different temperatures

The above results suggest that temperature can influence the response of the SARS-CoV-2 S glycoprotein to a one-hour exposure to soluble ACE2. This prompted us to evaluate the effect of temperature on the long-term stability of the ligand-free SARS-CoV-2 variant S glycoproteins. We incubated VSV vectors pseudotyped with the D614 and variant S glycoproteins at either 0°C (on ice), 4°C, RT, or 37°C for various periods of time before measuring their infectivity on Vero-E6 (Figures 5A and S2A, left) and 293T-ACE2 cells (Figures 5B and S2A, right). The infectivity of the VSV vectors pseudotyped by the variant S glycoproteins declined faster at 37°C than at RT, with little difference among the viruses with S glycoprotein variants at these temperatures. Viruses retained from 20 to 40 percent of their infectivity even after three days at RT. By contrast, incubation on ice or at 4°C revealed significant differences in the decay of infectivity among the viruses pseudotyped with the different SARS-CoV-2 S glycoproteins. Among the variants, B.1.1.7 was the most stable at 0 and 4°C, whereas P.1 and B.1.1.248 were inactivated at these temperatures more rapidly than the others. The D614, D614G, and B.1.351 exhibited intermediate levels of stability on ice and at 4°C. The S glycoproteins appear to be the major determinant of the loss of infectivity of the pseudotyped VSV as a result of incubation at 0 and 4°C, and significant differences in cold sensitivity exist among the S glycoproteins of the emerging SARS-CoV-2 variants.

As the cold sensitivity of the SARS-CoV-2 variants could hypothetically be related to the shedding of the S1 glycoprotein from the S trimer, we incubated each of the VSV pseudotypes on ice, at 4°C, at RT, and at 37°C for two days and then quantified S1 shedding from the viral particles (Figures 5C, 5D and S2B). The S1/S2 ratio for each SARS-CoV-2 variant is summarized in Figure 5E, with a lower ratio indicating greater S1 shedding. Spontaneous S1 shedding at 0 and 4°C for D614, P.1, and B.1.1.248 was significantly greater than that of D614G, B.1.1.7, and B.1.351. The higher rate of S1 shedding for P.1 and B.1.1.248 on ice and at 4°C likely contributes to their lower infectivity after prolonged incubation in the cold (Figures 5A, 5B, and S2A). Conversely, the B.1.1.7 variant was relatively resistant to spontaneous S1 shedding at 0 and 4°C, which is consistent with its higher infectivity after prolonged exposure to cold temperatures (Figures 5A, 5B, and S2A). D614, D614G, and B.1.351 were inactivated similarly on ice and at 4°C, but exhibited different levels of S1 shedding, suggesting that cold inactivation involves additional factors besides S1 shedding. With the exception of D614G, S1 shedding for each S glycoprotein variant was less at RT and 37°C than on ice. Collectively, these results suggest that factors in addition to S1 shedding can affect the infectivity of the variant S-pseudotyped viruses exposed to different temperatures.

We evaluated the effect of cold temperature on the infectivity and composition of authentic SARS-CoV-2 variants. The B.1.1.7 SARS-CoV-2 variant retained infectivity at 4°C better than the D614G and P.1 variants (Figure 5F). As was seen for the VSV pseudotypes, the authentic P.1 SARS-CoV-2 variant exhibited more S1 shedding over time at 4°C than the D614G and B.1.1.7 variants (Figure 5G). Thus, authentic SARS-CoV-2 variants exhibit differences in sensitivity to cold exposure.

Some SARS-CoV-2 variants are more resistant to convalescent COVID-19 patient sera and vaccinee sera

As we observed differences among the relative infectivity of the S glycoprotein variants when different levels of ACE2 were expressed on target cells, we hypothesized that the choice of target cells might also differentially affect antibody neutralization. We used Vero-E6 and 293T-ACE2 cells (shown in Figures 3C and 3D to have moderate and high levels of ACE2, respectively) as target cells in the neutralization assays. We tested the
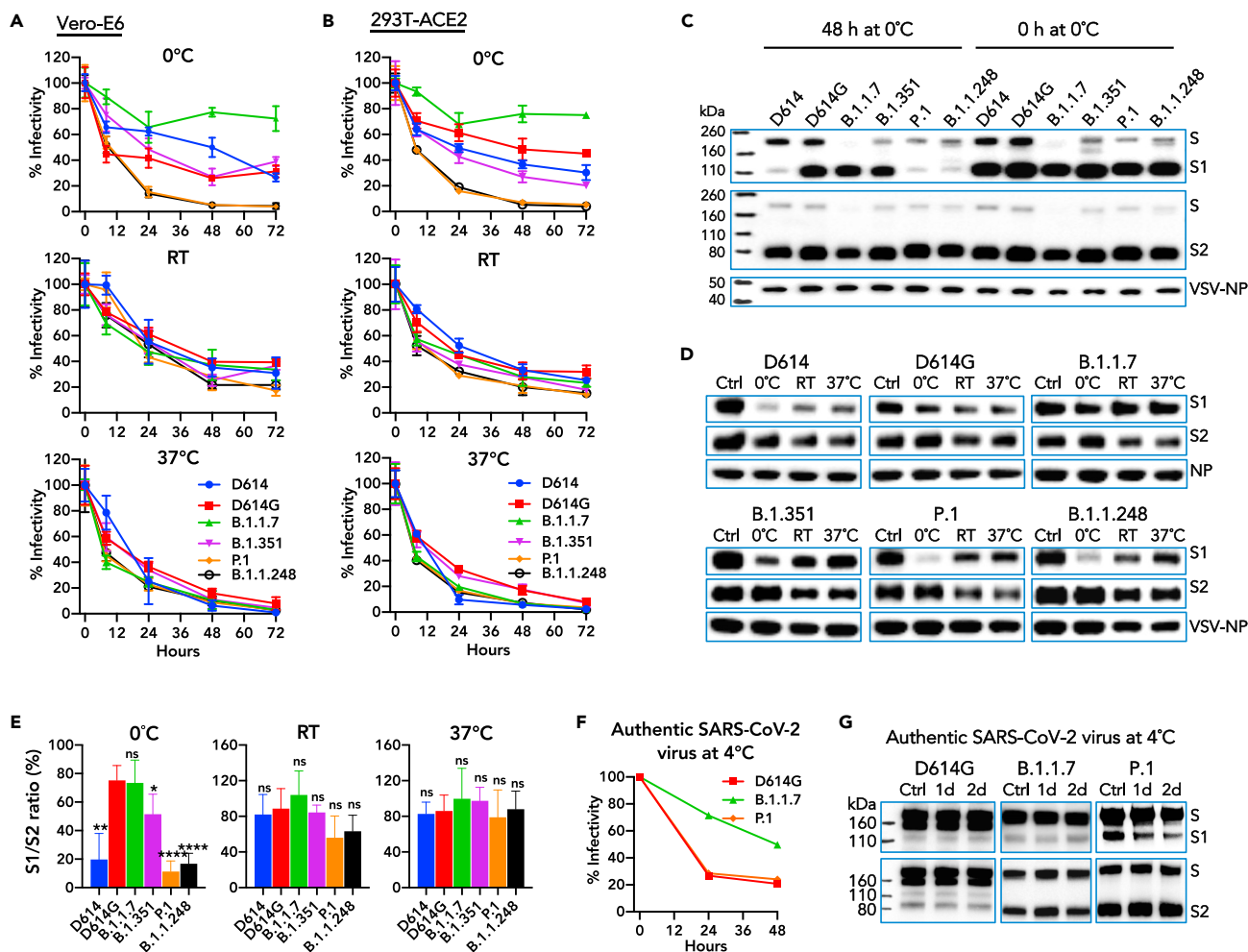
Figure 5. Stability of SARS-CoV-2 variants at different temperatures

(A and B) VSV vectors pseudotyped by the variant SARS-CoV-2 S glycoproteins were incubated on ice (upper panels), at room temperature (RT) (middle panels), and at 37°C (lower panels) for various times. The infectivity of the viruses was measured on Vero-E6 cells (A) and 293T-ACE2 cells (B). The infectivity at each time point is reported, relative to that observed at time 0 for each pseudovirus. Means and standard deviations derived from three replicates are shown. The results are representative of those obtained in three independent experiments. See also Figure S2A.
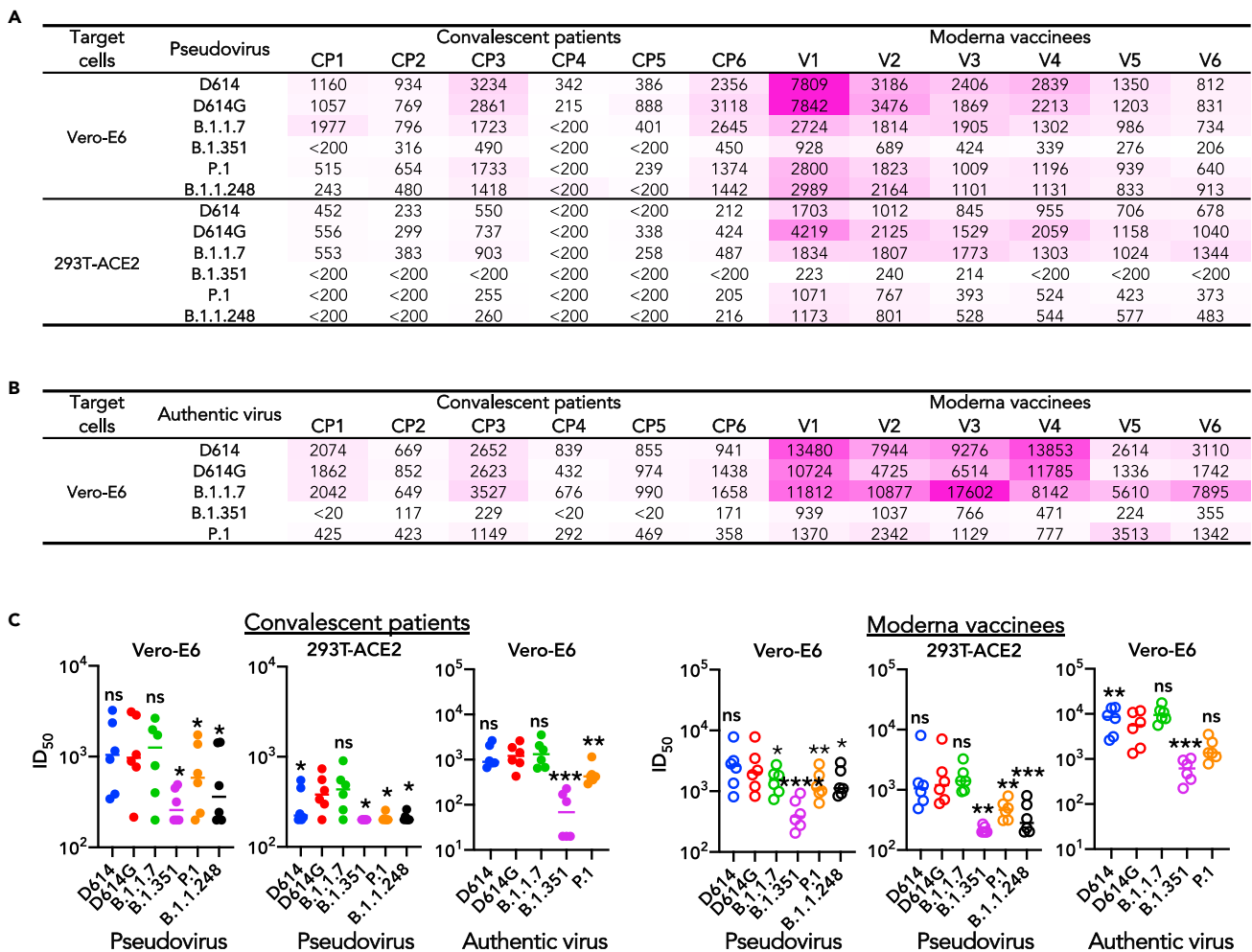
(C and D) VSV particles pseudotyped with the variant SARS-CoV-2 S glycoproteins were incubated on ice (C) or at the indicated temperatures (D) for 48 h. Pelleted VSV particles were analyzed by Western blotting with antibodies against S1, S2, and VSV NP. In (D), VSV pseudotypes that were not exposed to the different temperatures for 48 h served as controls (Ctrl). The results shown are representative of those obtained in three independent experiments. See also Figure S2B.

(E) The intensities of the S1 and S2 glycoprotein bands in (D) were measured. The S1/S2 ratios are shown for each variant relative to the ratio for the control sample of the pseudoviruses. The means and standard deviations derived from three independent experiments are shown. The S1/S2 ratio for each variant was compared with that of D614G. Statistical significance was evaluated with a Student's t test (*$p < 0.05$; **$p < 0.01$; ****$p < 0.0001$; ns – not significant).

(F) Authentic SARS-CoV-2 variants were incubated at 4°C for various times. The infectivity of the viruses was measured on Vero-E6 cells. The infectivity at each time point is reported, relative to that observed at time 0 for each virus variant. See also Figure S2A.

(G) Authentic SARS-CoV-2 variants were incubated at 4°C for 1 day and 2 days. Pelleted viral particles were analyzed by Western blotting with antibodies against S1 and S2. Viruses that were not exposed to 4°C served as controls (Ctrl). See also Figure S2B.

neutralization of VSV pseudotypes and authentic SARS-CoV-2 variants by two groups of sera: (1) sera collected from March to June 2020 from convalescent COVID-19 patients from New York City (Table S1) and (2) sera from individuals fully vaccinated with two doses of the Moderna COVID-19 vaccine. Both sets of sera recognized a SARS-CoV-2 S2P trimer; the titers of trimer-reactive antibodies were, on average, higher in the vaccinees than in patients with COVID-19 (Figure S3). In general, the neutralization titers of the sera were higher for Vero-E6 cells compared with those for 293T-ACE2 cells (Figures 6, S4, and S5). Qualitatively, the patterns of neutralization in the two target cells were similar. Consistent with other studies (Wang et al., 2021a, 2021b, 2021c), the sera

A

Target cells	Pseudovirus	Convalescent patients						Moderna vaccinees					
		CP1	CP2	CP3	CP4	CP5	CP6	V1	V2	V3	V4	V5	V6
Vero-E6	D614	1160	934	3234	342	386	2356	7809	3186	2406	2839	1350	812
	D614G	1057	769	2861	215	888	3118	7842	3476	1869	2213	1203	831
	B.1.1.7	1977	796	1723	<200	401	2645	2724	1814	1905	1302	986	734
	B.1.351	<200	316	490	<200	<200	450	928	689	424	339	276	206
	P.1	515	654	1733	<200	239	1374	2800	1823	1009	1196	939	640
	B.1.1.248	243	480	1418	<200	<200	1442	2989	2164	1101	1131	833	913
293T-ACE2	D614	452	233	550	<200	<200	212	1703	1012	845	955	706	678
	D614G	556	299	737	<200	338	424	4219	2125	1529	2059	1158	1040
	B.1.1.7	553	383	903	<200	258	487	1834	1807	1773	1303	1024	1344
	B.1.351	<200	<200	<200	<200	<200	<200	223	240	214	<200	<200	<200
	P.1	<200	<200	255	<200	<200	205	1071	767	393	524	423	373
	B.1.1.248	<200	<200	260	<200	<200	216	1173	801	528	544	577	483

B

Target cells	Authentic virus	Convalescent patients						Moderna vaccinees					
		CP1	CP2	CP3	CP4	CP5	CP6	V1	V2	V3	V4	V5	V6
Vero-E6	D614	2074	669	2652	839	855	941	13480	7944	9276	13853	2614	3110
	D614G	1862	852	2623	432	974	1438	10724	4725	6514	11785	1336	1742
	B.1.1.7	2042	649	3527	676	990	1658	11812	10877	17602	8142	5610	7895
	B.1.351	<20	117	229	<20	<20	171	939	1037	766	471	224	355
	P.1	425	423	1149	292	469	358	1370	2342	1129	777	3513	1342

C

Figure 6. Neutralization sensitivity of SARS-CoV-2 variants

(A) The serum neutralization titers (ID$_{50}$) of convalescent patient sera (CP1-CP6) and Moderna vaccinee sera (V1-V6) against VSV particles pseudotyped by the variant SARS-CoV-2 S glycoproteins are reported. The infectivity of the viruses was measured on Vero-E6 cells and 293T-ACE2 cells. The intensity of shading is proportionate to the potency of neutralizing activity. The results shown are representative of those obtained in two independent experiments. See also Table S1, Figures S3 and S4.

(B) The serum neutralization titers (ID$_{50}$) of convalescent patient sera (CP1-CP6) and Moderna vaccinee sera (V1-V6) against authentic SARS-CoV-2 variants are reported. The infectivity of the viruses was measured on Vero-E6 cells. The intensity of shading is proportionate to the potency of neutralizing activity. See also Figure S5.

(C) Serum neutralization ID$_{50}$ values of convalescent patient sera and Moderna vaccinee sera against VSV pseudoviruses (A) and authentic SARS-CoV-2 variants (B) were compared with those against D614G. Statistical analysis was performed using a paired t test (*p < 0.05; **p < 0.01; ***p < 0.001; and ****p < 0.0001; ns – not significant).

neutralized the B.1.1.7 variant as efficiently as D614 and D614G. By comparison, the neutralizing potency of these sera against B.1.351 was significantly diminished. The neutralization titers of the sera against the P.1 and B.1.1.248 variants were lower than those against D614G. These results are consistent with a recent report suggesting that South African and Brazilian SARS-CoV-2 variants are less susceptible to neutralization by plasma from German patients with COVID-19 (Hoffmann et al., 2021). Thus, the changes in the B.1.351, P.1, and B.1.1.248 S glycoproteins allow various levels of escape from some neutralizing antibodies elicited during natural SARS-CoV-2 infection or by vaccination.

DISCUSSION

The constant genetic evolution of viruses challenges the development of preventive measures and treatments. Newly emerging variants of SARS-CoV-2 with enhanced transmissibility and/or pathogenicity

SARS-CoV-2 S glycoprotein	Processing index	S1/S2 on pseudovirus	Cell-cell fusion	Relative infectivity		sACE2-Fc affinity (EC$_{50}$, nM)	sACE2.v2.4 Sensitivity (IC$_{50}$, nM)	sACE2-induced S1 shedding		Half-life of infectivity (hr)				S1/S2 ratio			Sensitivity to neutralizing antisera (average ID$_{50}$)					
										Pseudovirus			Authentic virus				Pseudovirus				Authentic virus	
																	Convalescent patients		Moderna vaccinees		Convalescent patients	Moderna vaccinees
				Low ACE2	High ACE2			0°C	37°C	0°C	RT	37°C	4°C	0°C	RT	37°C	Vero-E6	293T-ACE2	Vero-E6	293T-ACE2	Vero-E6	
D614	1	1	1	1	1	ND	0.91	1	1	24	24	12	ND	1	1	1	1402	308	3067	983	3239	8380
D614G	1.7	1	0.9	2.6	2.1	29.6	1.08	4.17	4	48	24	12	14	3.8	1.1	1	1485	426	2906	2022	2841	6138
B.1.1.7	0.5	1.3	0.9	3.3	1.8	3.6	0.47	0.25	1	>72	24	12	44	3.7	1.3	1.2	1290	464	1578	1514	3219	10323
B.1.351	1.2	0.9	1	5.2	1.5	17.5	0.47	10	4	20	24	12	ND	2.6	1	1.2	309	<200	477	213	249	632
P.1	0.9	0.8	1.1	11.4	2.7	9.4	0.24	0.25	4	8	24	12	14	0.6	0.7	1	786	<210	1401	592	677	1746
B.1.1.248	0.7	0.9	0.9	11.7	2.5	10.6	0.35	0.25	4	8	24	12	ND	0.8	0.8	1.1	664	<213	1522	684	ND	ND

Effect of changes   Down ▭▭▭ Up

Figure 7. Summary of phenotypes of the SARS-CoV-2 S glycoprotein variants
The primary data shown in Figures 1, 3, 4, 5, and 6 were used to calculate average values relative to those obtained for the D614 S glycoprotein. Decreases in the phenotypes relative to those of D614 are shaded red to a degree dependent on the level of the decrease. Increases in the phenotypes relative to those of D614 are shaded blue to a degree dependent on the level of the increase.

potentially drive local or global surges in prevalence. In this study, we compared the functional properties of the S glycoproteins of emerging SARS-CoV-2 variants with those of the original/founder D614 strain and the globally dominant D614G variant. The emerging variant S glycoproteins demonstrated increased ability to support virus entry into cells with low levels of the ACE2 receptor, differences in physical and functional S stability following exposure to the cold, and variation in sensitivity to neutralizing antisera. The phenotypes of the SARS-CoV-2 S glycoprotein variants are summarized in Figure 7.

Proteolytic cleavage of the variant S glycoprotein precursors, which are decorated with high-mannose carbohydrates, occurs in the Golgi, as evidenced by the extensive modification of the cleaved S1 and S2 glycoproteins by complex glycans. For all variants, we observed enrichment of the cleaved S1 and S2 glycoproteins in the pseudovirus particles compared with cell lysates. Thus, most of the S glycoproteins incorporated into VSV or lentiviral particles have passed through the Golgi apparatus.

The infectivity of viruses pseudotyped with all of the variant S glycoproteins increased with higher levels of expression of the ACE2 receptor on the target cells. At low target cell ACE2 levels, the relative ability of the different SARS-CoV-2 S glycoproteins to mediate virus entry exhibited the following rank order: P.1, B.1.1.248 > B.1.351 > B.1.1.7 > D614G > D614. Improved interaction with ACE2 and/or better triggering following ACE2 binding likely contribute to the ability of the emerging variant S glycoproteins to utilize lower levels of target cell ACE2. Supporting this assertion are the observed increases in the affinity of B.1.1.7, B.1.351, P.1, and B.1.1.248 soluble S glycoprotein trimers for ACE2 and the greater sensitivity of viruses pseudotyped with these S variants to dimeric soluble ACE2. Increased sensitivity to soluble ACE2 has been attributed to the N501Y change found in the RBD of the B.1.1.7, B.1.351, P.1, and B.1.1.248 S glycoproteins (Tian et al., 2021). As ACE2 expression levels vary depending on the location and differentiation state of human airway epithelial cells (Jia et al., 2005; Ortiz et al., 2020), the ability to support infection of cells with low ACE2 potentially enhances the tropism, transmission, and/or pathogenicity of SARS-CoV-2 variants.

The infectivity of VSV vectors pseudotyped by the variant S glycoproteins decayed equivalently at RT and 37°C, with half-lives of approximately 24 and 12 h, respectively. These half-lives are much shorter than the reported half-life of infectious VSV (28 and 7 days at RT and 37°C, respectively) (Zimmer et al., 2013); therefore, functional inactivation of the SARS-CoV-2 S glycoproteins on the VSV pseudotypes likely is the predominant determinant of the observed loss of infectivity at these temperatures. Spontaneous S1 shedding from the S glycoprotein was apparently not required for functional inactivation at RT or 37°C, given the significant amount of S1 remaining on the virus particles after 48 h at these temperatures.

Intriguing differences among the phenotypes of the emerging SARS-CoV-2 variant S glycoproteins were revealed in the cold. Incubation on ice or at 4°C led to rapid loss of infectivity of P.1 and B.1.1.248 pseudotypes, in comparison to the D614, D614G, and B.1.351 viruses. In contrast, the infectivity of the B.1.1.7 pseudotype was more stable at 0 and 4°C than that of the other viruses. Likewise, the authentic B.1.1.7 SARS-CoV-2 variant exhibited a longer half-life at 4°C than the authentic D614G and P.1 variants. We found that the incubation of the pseudotyped viruses on ice or at 4°C led to a dramatic loss of the S1 glycoprotein from the P.1 and B.1.1.248 S trimers, whereas the B.1.1.7 S glycoprotein was minimally affected under the same conditions. These results suggest that the differential destabilization of the variant S glycoprotein trimers

leading to S1 shedding contributes to the observed inactivation of virus infectivity in the cold. However, we note that, as previously seen (Nguyen et al., 2020), the D614G S is more stable and sheds S1 less at 0 or 4°C than the D614 S, yet these two variants exhibit minimal differences in the rate of decay of infectivity at these temperatures. Apparently, maintaining an intact S glycoprotein trimer after prolonged exposure to cold temperatures is not sufficient for the retention of S function.

Some oligomeric proteins undergo denaturation at temperatures near 0°C as a result of the weakening of intersubunit interactions (Lopez et al., 2008; Privalov, 1990; Tsai et al., 2002). For example, HIV-1 infectivity can be attenuated by incubation on ice, and the different sensitivities of HIV-1 strains to cold inactivation are determined by their envelope glycoproteins (Kassa et al., 2009a; Medjahed et al., 2013). Although the cold denaturation of some proteins is reversible, cold-induced changes in high-potential-energy, meta-stable viral envelope glycoproteins typically lead to irreversible transitions to low-energy states incapable of mediating membrane fusion. Of interest, the sensitivity of HIV-1 strains to cold is related to the propensity of their envelope glycoproteins to make the transition from the pretriggered conformation to the receptor-bound conformation (Kassa et al., 2009b). If the sensitivity of the P.1 and B.1.1.248 variants to cold inactivation likewise indicates an increased propensity to sample receptor-bound conformations, this tendency could contribute to the higher relative infectivity of these variants on cells with low ACE2 levels. Indeed, HIV-1 envelope glycoprotein mutants with changes that destabilize the pretriggered conformation are better able to support virus entry into cells with low levels of the CD4 receptor (Haim et al., 2011; Herschhorn et al., 2016).

The ability to withstand low temperatures could have practical value for a respiratory virus that is horizontally transmitted by aerosols/droplets and is potentially exposed to a range of environmental conditions. Although naturally transmitted SARS-CoV-2 is not typically exposed to near-freezing temperatures for prolonged periods of time, cold resistance is a surrogate indicator of the ability of the functional viral S glycoprotein trimer to resist conformational changes induced by various forms of environmental stress (Lopez et al., 2008; Privalov, 1990; Tsai et al., 2002). For example, as a virus transmitted by sexual or blood contacts, HIV-1 is not naturally exposed to cold temperatures; nonetheless, viruses with cold-sensitive HIV-1 envelope glycoproteins revert to cold-resistant forms in vivo, at least in part because the latter envelope glycoproteins elicit less effective host antibody responses (McGee et al., 2014). It is possible that local climate might influence the evolution of SARS-CoV-2 variants differing in the stability of the functional S glycoprotein trimer. The B.1.1.7, B.1.351, P.1, and B.1.1.248 SARS-CoV-2 variants all evolved from D614G, which exhibits an increase in S stability at low temperatures relative to D614, but is still inactivated functionally by extended exposure to cold (Nguyen et al., 2020). The B.1.1.7 variant, which retains S stability and infectivity in the cold, is becoming dominant in countries with a range of climates. B.1.351, P.1, and B.1.1.248 emerged in the more temperate climates of South Africa and Brazil, where resistance to cold-related stress may be less valuable to the success of the virus. It will be interesting to compare the spread and evolution of the closely related P.1 and B.1.1.248 variants in Brazil and climatically diverse Japan, respectively.

We examined the sensitivity of authentic SARS-CoV-2 variants, as well as VSV vectors pseudotyped by the variant S glycoproteins, to neutralization by sera from convalescent COVID-19 patients and recipients of the Moderna COVID-19 vaccine. The neutralization profile of B.1.1.7 was similar to that of D614 and D614G, whereas B.1.351, P.1, and B.1.1.248 were less sensitive to these antisera. The K417N and E484K changes in the S1 RBD have been shown to contribute to escape from neutralizing antibodies (Chen et al., 2021; Wang et al., 2021a, 2021b, 2021c). We found that serum neutralization was generally more effective with target cells that express lower levels of ACE2. This supports the notion that ACE2 receptors on the target cell and many neutralizing antibodies compete for binding to the S1 RBD.

Differing abilities of the S glycoprotein variants to utilize low levels of the target cell receptor, to maintain structural and functional integrity in the cold, and to resist host neutralizing antibodies potentially contribute to the adaptation of emerging SARS-CoV-2 variants to their environments. Understanding these aspects of SARS-CoV-2 S biology should assist attempts to control the COVID-19 pandemic.

Limitations of the study

Additional studies of variant S glycoprotein phenotypes in the context of authentic SARS-CoV-2 would be valuable. Mapping the S glycoprotein determinants of the observed phenotypes could provide insights into structure–function relationships. The effect of colder temperatures on the stability of the virion S glycoprotein trimer could be further assessed at the population level, where the efficiency of transmission of

certain variants of concern might demonstrate a dependence on the local climate. Since the completion of this work, multiple additional SARS-CoV-2 variants of concern have arisen. Similar studies of the function of these variant S glycoproteins might identify determinants of transmissibility and pathogenesis. For example, the S glycoprotein of the currently dominant B.1.617.2 variant (delta) has a cleavage site alteration that is suggested to contribute to efficient cleavage and increased virus infectivity (Liu et al., 2021).

STAR★METHODS

Detailed methods are provided in the online version of this paper and include the following:

- KEY RESOURCES TABLE
- RESOURCE AVAILABILITY
  - Lead contact
  - Materials availability
  - Data and code availability
- EXPERIMENTAL MODEL AND SUBJECT DETAILS
  - Human subjects
  - Cell lines
- METHOD DETAILS
  - Plasmid constructs
  - Expression and purification of protein reagents
  - VSV pseudotyped by SARS-CoV-2 S glycoproteins
  - Lentiviruses pseudotyped by SARS-CoV-2 S glycoproteins
  - S glycoprotein expression, processing, and incorporation into pseudovirus particles
  - Deglycosylation of S glycoproteins
  - Virus infectivity and stability at different temperatures
  - Cell-cell fusion assays
  - Spike trimer ELISA
  - S1 shedding from spike trimers
  - Neutralization assay
- QUANTIFICATION AND STATISTICAL ANALYSIS

SUPPLEMENTAL INFORMATION

Supplemental information can be found online at https://doi.org/10.1016/j.isci.2021.103393.

AUTHOR CONTRIBUTIONS

Q.W. and J.G.S. designed the research. Q.W., M.S.N., S.A., S.Z., L.L., and Y.H. performed the experimental work. Specifically, Q.W. performed all the experiments except the soluble ACE2 and spike trimer preparation, and the assays involving authentic SARS-CoV-2 variants. S.A. performed the alpha complementation assays and soluble ACE2-induced S1 shedding assays. S.Z. purified the soluble ACE2 protein. L.L. and D.D.H. provided the convalescent and vaccinee sera, soluble spike trimers, sACE2-Fc, and sACE2.v2.4. M.S.N., L.L., and Y.H. performed the assays involving authentic SARS-CoV-2 variants. J.G.S. and H.T.N. directed the research and provided guidance. Q.W., S.A., H.T.N., and J.G.S. analyzed the data and wrote the manuscript. All authors reviewed and edited the manuscript.

DECLARATION OF INTERESTS

The authors declare no competing interests.

REFERENCES

Anderson, E.J., Rouphael, N.G., Widge, A.T., Jackson, L.A., Roberts, P.C., Makhene, M., Chappell, J.D., Denison, M.R., Stevens, L.J., Pruijssers, A.J., et al. (2020). Safety and immunogenicity of SARS-CoV-2 mRNA-1273 vaccine in older adults. N. Engl. J. Med. 383, 2427–2438.

AstraZeneca (2021). AZD1222 US Phase III Trial Met Primary Efficacy Endpoint in Preventing COVID-19 at Interim Analysis.

Baden, L.R., El Sahly, H.M., Essink, B., Kotloff, K., Frey, S., Novak, R., Diemert, D., Spector, S.A., Rouphael, N., Creech, C.B., et al. (2021). Efficacy and safety of the mRNA-1273 SARS-CoV-2 vaccine. N. Engl. J. Med. 384, 403–416.

Bosch, B.J., van der Zee, R., de Haan, C.A., and Rottier, P.J. (2003). The coronavirus spike protein is a class I virus fusion protein: structural and functional characterization of the fusion core complex. J. Virol. 77, 8801–8811.

CDC, C.f.D.C.a.P. (2021). Science Brief: Emerging SARS-CoV-2 Variants.

Chan, K.K., Dorosky, D., Sharma, P., Abbasi, S.A., Dye, J.M., Kranz, D.M., Herbert, A.S., and Procko, E. (2020). Engineering human ACE2 to optimize binding to the spike protein of SARS coronavirus 2. Science 369, 1261–1265.

Chen, R.E., Zhang, X., Case, J.B., Winkler, E.S., Liu, Y., VanBlargan, L.A., Liu, J., Errico, J.M., Xie, X., Suryadevara, N., et al. (2021). Resistance of SARS-CoV-2 variants to neutralization by monoclonal and serum-derived polyclonal antibodies. Nat. Med. 27, 717–726.

Davies, N.G., Abbott, S., Barnard, R.C., Jarvis, C.I., Kucharski, A.J., Munday, J.D., Pearson, C.A.B., Russell, T.W., Tully, D.C., Washburne, A.D., et al. (2021a). Estimated transmissibility and impact of SARS-CoV-2 lineage B.1.1.7 in England. Science 372, eabg3055.

Davies, N.G., Jarvis, C.I., Group, C.C.-W., Edmunds, W.J., Jewell, N.P., Diaz-Ordaz, K., and Keogh, R.H. (2021b). Increased mortality in community-tested cases of SARS-CoV-2 lineage B.1.1.7. Nature 593, 270–274.

du Plessis, L., McCrone, J.T., Zarebski, A.E., Hill, V., Ruis, C., Gutierrez, B., Raghwani, J., Ashworth, J., Colquhoun, R., Connor, T.R., et al. (2021). Establishment and lineage dynamics of the SARS-CoV-2 epidemic in the UK. Science 371, 708–712.

Fujino, T., Nomoto, H., Kutsuna, S., Ujiie, M., Suzuki, T., Sato, R., Fujimoto, T., Kuroda, M., Wakita, T., and Ohmagari, N. (2021). Novel SARS-CoV-2 variant in travelers from Brazil to Japan. Emerg. Infect. Dis. 27, 1243–1245.

Gobeil, S.M., Janowska, K., McDowell, S., Mansouri, K., Parks, R., Stalls, V., Kopp, M.F., Manne, K., Li, D., Wiehe, K., et al. (2021). Effect of natural mutations of SARS-CoV-2 on spike structure, conformation, and antigenicity. Science 373, eabi6226.

Haim, H., Strack, B., Kassa, A., Madani, N., Wang, L., Courter, J.R., Princiotto, A., McGee, K., Pacheco, B., Seaman, M.S., et al. (2011). Contribution of intrinsic reactivity of the HIV-1 envelope glycoproteins to CD4-independent infection and global inhibitor sensitivity. Plos Pathog. 7, e1002101.

Herschhorn, A., Ma, X., Gu, C., Ventura, J.D., Castillo-Menendez, L., Melillo, B., Terry, D.S., Smith, A.B., 3rd, Blanchard, S.C., Munro, J.B., et al. (2016). Release of gp120 Restraints leads to an entry-Competent intermediate state of the HIV-1 envelope glycoproteins. mBio 7, e01598–01516.

Hoffmann, M., Arora, P., Gross, R., Seidel, A., Hornich, B.F., Hahn, A.S., Kruger, N., Graichen, L., Hofmann-Winkler, H., Kempf, A., et al. (2021). SARS-CoV-2 variants B.1.351 and P.1 escape from neutralizing antibodies. Cell 184, 2384–2393 e12.

Hu, B., Guo, H., Zhou, P., and Shi, Z.L. (2021). Characteristics of SARS-CoV-2 and COVID-19. Nat. Rev. Microbiol. 19, 141–154.

Isho, B., Abe, K.T., Zuo, M., Jamal, A.J., Rathod, B., Wang, J.H., Li, Z., Chao, G., Rojas, O.L., Bang, Y.M., et al. (2020). Persistence of serum and saliva antibody responses to SARS-CoV-2 spike antigens in COVID-19 patients. Sci. Immunol. 5, eabe5511.

Jia, H.P., Look, D.C., Shi, L., Hickey, M., Pewe, L., Netland, J., Farzan, M., Wohlford-Lenane, C., Perlman, S., and McCray, P.B., Jr. (2005). ACE2 receptor expression and severe acute respiratory syndrome coronavirus infection depend on differentiation of human airway epithelia. J. Virol. 79, 14614–14621.

Johnson, J. (2021). Johnson & Johnson Announces Single-Shot Janssen COVID-19 Vaccine Candidate Met Primary Endpoints in Interim Analysis of its Phase 3 ENSEMBLE Trial.

Kassa, A., Finzi, A., Pancera, M., Courter, J.R., Smith, A.B., 3rd, and Sodroski, J. (2009a). Identification of a human immunodeficiency virus type 1 envelope glycoprotein variant resistant to cold inactivation. J. Virol. 83, 4476–4488.

Kassa, A., Madani, N., Schon, A., Haim, H., Finzi, A., Xiang, S.H., Wang, L., Princiotto, A., Pancera, M., Courter, J., et al. (2009b). Transitions to and from the CD4-bound conformation are modulated by a single-residue change in the human immunodeficiency virus type 1 gp120 inner domain. J. Virol. 83, 8364–8378.

Korber, B., Fischer, W.M., Gnanakaran, S., Yoon, H., Theiler, J., Abfalterer, W., Hengartner, N., Giorgi, E.E., Bhattacharya, T., Foley, B., et al. (2020). Tracking changes in SARS-CoV-2 spike: evidence that D614G increases infectivity of the COVID-19 virus. Cell 182, 812–827 e819.

Krammer, F. (2020). SARS-CoV-2 vaccines in development. Nature 586, 516–527.

Kupferschmidt, K. (2021). Fast-spreading U.K. virus variant raises alarms. Science 371, 9–10.

Laffeber, C., de Koning, K., Kanaar, R., and Lebbink, J.H.G. (2021). Experimental evidence for enhanced receptor binding by rapidly spreading SARS-CoV-2 variants. J. Mol. Biol. 433, 167058.

Li, Q., Wu, J., Nie, J., Zhang, L., Hao, H., Liu, S., Zhao, C., Zhang, Q., Liu, H., Nie, L., et al. (2020). The impact of mutations in SARS-CoV-2 spike on viral infectivity and antigenicity. Cell 182, 1284–1294.e1289.

Liu, Y., Liu, J., Johnson, B.A., Xia, H., Ku, Z., Schindewolf, C., Widen, S.G., An, Z., Weaver, S.C., Menachery, V.D., et al. (2021). Delta spike P681R mutation enhances SARS-CoV-2 fitness over Alpha variant. bioRxiv, 2021.08.12.456173.

Liu, L., Wang, P., Nair, M.S., Yu, J., Rapp, M., Wang, Q., Luo, Y., Chan, J.F., Sahi, V., Figueroa, A., et al. (2020). Potent neutralizing antibodies against multiple epitopes on SARS-CoV-2 spike. Nature 584, 450–456.

Lopez, C.F., Darst, R.K., and Rossky, P.J. (2008). Mechanistic elements of protein cold denaturation. J. Phys. Chem. B 112, 5961–5967.

McGee, K., Haim, H., Korioth-Schmitz, B., Espy, N., Javanbakht, H., Letvin, N., and Sodroski, J. (2014). The selection of low envelope glycoprotein reactivity to soluble CD4 and cold during simian-human immunodeficiency virus infection of rhesus macaques. J. Virol. 88, 21–40.

Medjahed, H., Pacheco, B., Desormeaux, A., Sodroski, J., and Finzi, A. (2013). The HIV-1 gp120 major variable regions modulate cold inactivation. J. Virol. 87, 4103–4111.

National Institute of Infectious Diseases, J. (2021). Brief Report: New Variant Strain of SARS-CoV-2 Identified in Travelers from Brazil.

Ng, W.H., Liu, X., and Mahalingam, S. (2020). Development of Vaccines for SARS-CoV-2. F1000Res 9, F1000 Faculty Rev-1991.

Nguyen, H.T., Zhang, S., Wang, Q., Anang, S., Wang, J., Ding, H., Kappes, J.C., and Sodroski, J. (2020). Spike glycoprotein and host cell determinants of SARS-CoV-2 entry and cytopathic effects. J. Virol. 95, e02304–02320.

Nicola, M., Alsafi, Z., Sohrabi, C., Kerwan, A., Al-Jabir, A., Iosifidis, C., Agha, M., and Agha, R. (2020). The socio-economic implications of the coronavirus pandemic (COVID-19): a review. Int. J. Surg. 78, 185–193.

Novavax (2021). Novavax COVID-19 Vaccine Demonstrates 89.3% Efficacy in UK Phase 3 Trial.

Ortiz, M.E., Thurman, A., Pezzulo, A.A., Leidinger, M.R., Klesney-Tait, J.A., Karp, P.H., Tan, P., Wohlford-Lenane, C., McCray, P.B., Jr., and Meyerholz, D.K. (2020). Heterogeneous expression of the SARS-Coronavirus-2 receptor ACE2 in the human respiratory tract. EBioMedicine 60, 102976.

Polack, F.P., Thomas, S.J., Kitchin, N., Absalon, J., Gurtman, A., Lockhart, S., Perez, J.L., Perez Marc, G., Moreira, E.D., Zerbini, C., et al. (2020). Safety and efficacy of the BNT162b2 mRNA Covid-19 vaccine. N. Engl. J. Med. 383, 2603–2615.

Privalov, P.L. (1990). Cold denaturation of proteins. Crit. Rev. Biochem. Mol. Biol. 25, 281–305.

Schmidt, F., Weisblum, Y., Muecksch, F., Hoffmann, H.H., Michailidis, E., Lorenzi, J.C.C., Mendoza, P., Rutkowska, M., Bednarski, E., Gaebler, C., et al. (2020). Measuring SARS-CoV-2 neutralizing antibody activity using pseudotyped

and chimeric viruses. J. Exp. Med. *217*, e20201181.

Tegally, H., Wilkinson, E., Giovanetti, M., Iranzadeh, A., Fonseca, V., Giandhari, J., Doolabh, D., Pillay, S., San, E.J., Msomi, N., et al. (2020). Emergence and rapid spread of a new severe acute respiratory syndrome-related coronavirus 2 (SARS-CoV-2) lineage with multiple spike mutations in South Africa. medRxiv, 2020.12.21.20248640v1.

Tian, F., Tong, B., Sun, L., Shi, S., Zheng, B., Wang, Z., Dong, X., and Zheng, P. (2021). N501Y mutation of spike protein in SARS-CoV-2 strengthens its binding to receptor ACE2. Elife *10*, e69091.

Tsai, C.J., Maizel, J.V., Jr., and Nussinov, R. (2002). The hydrophobic effect: a new insight from cold denaturation and a two-state water structure. Crit. Rev. Biochem. Mol. Biol. *37*, 55–69.

Volz, E., Hill, V., McCrone, J.T., Price, A., Jorgensen, D., O'Toole, A., Southgate, J., Johnson, R., Jackson, B., Nascimento, F.F., et al. (2021). Evaluating the effects of SARS-CoV-2 spike mutation D614G on transmissibility and pathogenicity. Cell *184*, 64–75 e11.

Voysey, M., Clemens, S.A.C., Madhi, S.A., Weckx, L.Y., Folegatti, P.M., Aley, P.K., Angus, B., Baillie, V.L., Barnabas, S.L., Bhorat, Q.E., et al. (2021). Safety and efficacy of the ChAdOx1 nCoV-19

vaccine (AZD1222) against SARS-CoV-2: an interim analysis of four randomised controlled trials in Brazil, South Africa, and the UK. Lancet *397*, 99–111.

Wang, L., Wang, Y., Ye, D., and Liu, Q. (2020). Review of the 2019 novel coronavirus (SARS-CoV-2) based on current evidence. Int. J. Antimicrob. Agents *55*, 105948.

Wang, P., Casner, R.G., Nair, M.S., Wang, M., Yu, J., Cerutti, G., Liu, L., Kwong, P.D., Huang, Y., Shapiro, L., et al. (2021a). Increased resistance of SARS-CoV-2 variant P.1 to antibody neutralization. Cell Host Microbe *29*, 747–751.e744.

Wang, P., Nair, M.S., Liu, L., Iketani, S., Luo, Y., Guo, Y., Wang, M., Yu, J., Zhang, B., Kwong, P.D., et al. (2021b). Antibody resistance of SARS-CoV-2 variants B.1.351 and B.1.1.7. Nature *593*, 130–135.

Wang, R., Zhang, Q., Ge, J., Ren, W., Zhang, R., Lan, J., Ju, B., Su, B., Yu, F., Chen, P., et al. (2021c). Analysis of SARS-CoV-2 variant mutations reveals neutralization escape mechanisms and the ability to use ACE2 receptors from additional species. Immunity *54*, 1611–1621.e1615.

Wang, Z., Schmidt, F., Weisblum, Y., Muecksch, F., Barnes, C.O., Finkin, S., Schaefer-Babajew, D., Cipolla, M., Gaebler, C., Lieberman, J.A., et al. (2021d). mRNA vaccine-elicited antibodies to

SARS-CoV-2 and circulating variants. Nature *592*, 616–622.

Wu, K., Werner, A.P., Koch, M., Choi, A., Narayanan, E., Stewart-Jones, G.B.E., Colpitts, T., Bennett, H., Boyoglu-Barnum, S., Shi, W., et al. (2021). Serum neutralizing activity elicited by mRNA-1273 vaccine. N. Engl. J. Med. *384*, 1468–1470.

Xia, S., Zhang, Y., Wang, Y., Wang, H., Yang, Y., Gao, G.F., Tan, W., Wu, G., Xu, M., Lou, Z., et al. (2021). Safety and immunogenicity of an inactivated SARS-CoV-2 vaccine, BBIBP-CorV: a randomised, double-blind, placebo-controlled, phase 1/2 trial. Lancet Infect. Dis. *21*, 39–51.

Zhang, L., Jackson, C.B., Mou, H., Ojha, A., Peng, H., Quinlan, B.D., Rangarajan, E.S., Pan, A., Vanderheiden, A., Suthar, M.S., et al. (2020). SARS-CoV-2 spike-protein D614G mutation increases virion spike density and infectivity. Nat. Commun. *11*, 6013.

Zhang, J., Cai, Y., Xiao, T., Lu, J., Peng, H., Sterling, S.M., Walsh, R.M., Jr., Rits-Volloch, S., Zhu, H., Woosley, A.N., et al. (2021). Structural impact on SARS-CoV-2 spike protein by D614G substitution. Science *372*, 525–530.

Zimmer, B., Summermatter, K., and Zimmer, G. (2013). Stability and inactivation of vesicular stomatitis virus, a prototype rhabdovirus. Vet. Microbiol. *162*, 78–84.

STAR★METHODS

KEY RESOURCES TABLE

REAGENT or RESOURCE	SOURCE	IDENTIFIER
Antibodies		
Rabbit anti-SARS-Spike S1	Sino Biological	Cat# 40591-T62; RRID:AB_2893171
Rabbit anti-SARS-Spike S2	Sino Biological	Cat# 40590-T62
Rabbit anti-p55/p24/p17	Abcam	Cat# ab63917; RRID:AB_1139524
Mouse anti-VSV-NP	Millipore	Cat# MABF2348
Mouse anti-GAPDH	Millipore	Cat# CB1001; RRID:AB_2107426
SARS-CoV-2 Nucleocapsid Protein Monoclonal Antibody (7E1B)	CliniSciences	Cat# bsm-41414M; RRID:AB_2848129
HRP-conjugated anti-Rabbit antibody	Cytiva	Cat# NA934-1ML; RRID:AB_2722659
HRP-conjugated goat anti-mouse antibody	Jackson ImmunoResearch	Cat# 115-035-008; RRID:AB_2313585
Goat anti-ACE2	R&D Systems	Cat# AF933; RRID:AB_355722
Alexa 488 conjugated Donkey anti-Goat	Invitrogen	Cat# A32814; RRID:AB_2762838
HRP-conjugated Mouse anti-Goat antibody	Invitrogen	Cat# 31400; RRID:AB_228370
Peroxidase AffiniPure goat anti-human IgG (H+L) antibody	Jackson ImmunoResearch	Cat# 109-035-003; RRID:AB_2337577
Bacterial and virus strains		
VSV-G pseudotyped ΔG-luciferase	Kerafast	Cat# EH1020-PM
Biological samples		
CP1-CP6 sera	(Wang et al., 2021a, 2021b)	N/A
V1-V6 sera	(Wang et al., 2021a, 2021b)	N/A
Chemicals, peptides, and recombinant proteins		
sACE2.v2.4	(Wang et al., 2021a, 2021b)	N/A
sACE2-Fc	(Wang et al., 2021a, 2021b)	N/A
sACE2-strep	This paper	N/A
SARS-CoV-2 D614G S2P	(Wang et al., 2021a, 2021b)	N/A
SARS-CoV-2 B.1.1.7 S2P	(Wang et al., 2021a, 2021b)	N/A
SARS-CoV-2 B.1.351 S2P	(Wang et al., 2021a, 2021b)	N/A
SARS-CoV-2 P.1 S2P	(Wang et al., 2021a, 2021b)	N/A
SARS-CoV-2 B.1.1.248 S2P	(Wang et al., 2021a, 2021b)	N/A
Critical commercial assays		
Pseudotyped ΔG-luciferase (G*ΔG-luciferase) rVSV	Kerafast	Cat# EH1025-PM
Luciferase Assay System	Promega	Cat# E4550
Galacto-Star™ Reaction Buffer Diluent with Galacton-Star™ Substrate	Thermo Fisher	Cat# T1056
PNGase F	NEB	Cat# P0704L
Endo Hf	NEB	Cat# P0703L
3, 3′,5 ,5′-Tetramethylbenzidine Liquid Substrate, Supersensitive, for ELISA	Sigma-Aldrich	Cat# T4444
Q5 Site-Directed Mutagenesis Kit	NEB	Cat# E0554S

Continued

REAGENT or RESOURCE	SOURCE	IDENTIFIER
Experimental models: Cell lines		
293T	ATCC	CRL-3216
293T-ACE2	BEI	NR-5211
Vero-E6	ATCC	CRL-1586
TZM-bl-ACE2	This paper	N/A
COS-1	ATCC	CRL-1650
Experimental models: Organisms/strains		
SARS-Related Coronavirus 2 Isolate USA-WA1/2020 (D614)	BEI Resources (NIAID, NIH)	NR-52281
SARS-Related Coronavirus 2 Isolate Germany/BavPat1/2020 (D614G)		NR-52370
SARS-Related Coronavirus 2 Isolate USA/CA_CDC_5574/2020 (B.1.1.7)		NR-54011
SARS-Related Coronavirus 2 Isolate hCoV-19/USA/MD-HP01542/2021 (B.1.351)		NR-54008
SARS-Related Coronavirus 2 Isolate hCoV-19/Japan/TY7-503/2021 (P.1)		NR-54982
Recombinant DNA		
Plasmid: SARS-CoV-2 D614 spike	Sino Biological	VG40589-UT(D614)
Plasmid: SARS-CoV-2 D614G spike	This paper	N/A
Plasmid: SARS-CoV-2 B.1.1.7 spike	This paper	N/A
Plasmid: SARS-CoV-2 B.1.351 spike	This paper	N/A
Plasmid: SARS-CoV-2 P.1 spike	This paper	N/A
Plasmid: SARS-CoV-2 B.1.1.248 spike	This paper	N/A
Plasmid: sACE2.v2.4	(Chan et al., 2020)	Addgene Plasmid #154106
pHIV-1$_{NL4-3}$ ΔEnv-NanoLuc	(Liu et al., 2020)	N/A
Plasmid: sACE2-strep	(Nguyen et al., 2020)	N/A
Plasmid: sACE2-Fc	This paper	N/A
Software and algorithms		
ImageJ	the National Institutes of Health	https://imagej.nih.gov/ij/
Image lab	Bio-rad	https://www.bio-rad.com/en-us/product/image-lab-software?ID=KRE6P5E8Z
GraphPad Prism 8	GraphPad Software Inc	https://www.graphpad.com/scientific-software/prism/
FlowJo 10	FlowJo LLC	https://www.flowjo.com/solutions/flowjo/downloads

RESOURCE AVAILABILITY

Lead contact

Further information and requests for resources and reagents should be directed to and will be fulfilled by the lead contact, Dr. Joseph G. Sodroski (joseph_sodroski@dfci.harvard.edu).

Materials availability

All requests for resources and reagents should be directed to and will be fulfilled by the Lead Contact, Dr. Joseph G. Sodroski (joseph_sodroski@dfci.harvard.edu). This includes selective cell lines, plasmids, antibodies, viruses, serum and proteins. All reagents will be made available on request after completion of a Material Transfer Agreement.

Data and code availability

Any additional information required to reanalyze the data reported in this paper is available from the lead contact upon request.

- Data

Data reported in this paper will be shared by the lead contact upon request.

- Code

This paper does not report original codes.

- All other items

Any additional information required to reanalyze the data reported in this paper is available from the lead contact upon request.

EXPERIMENTAL MODEL AND SUBJECT DETAILS

Human subjects

Plasma samples were obtained from patients (aged 27–85 years) convalescing from SARS-CoV-2 infection. The patients were enrolled into an observational cohort study of patients convalescing from COVID-19 at the Columbia University Irving Medical Center (CUIMC) starting in the spring of 2020. The study protocol was approved by the CUIMC Institutional Review Board (IRB) and all participants provided written informed consent. Detailed descriptions of convalescent patients enrolled in the study can be found in Table S1.

Sera were obtained from 6 participants in a phase-I clinical trial of the Moderna SARS-CoV-2 mRNA-1273 vaccine conducted at the NIH, under a NIH IRB-approved protocol (Anderson et al., 2020).

Cell lines

HEK293T, 293T-ACE2 (BEI), Vero-E6, TZM-bl-ACE2 and COS-1 cells were cultured in Dulbecco modified Eagle medium (DMEM) supplemented with 10% fetal bovine serum (FBS) and 100 μg/ml penicillin-streptomycin (Thermo Fisher Scientific, Cambridge, MA). Expi293 cells were maintained in suspension culture directly in Expi293™ Expression Medium, supplemented with penicillin and streptomycin and were incubated at 37°C in a humidified atmosphere of 8% CO_2 in air and on a shaker platform rotating at 125 rpm. HEK293T cells, 293T-ACE2 cells, TZM-bl-ACE2 cells, Expi293 cells are of female origin. Vero-E6 and COS-1 were from African green monkey kidney.

METHOD DETAILS

Plasmid constructs

The codon-optimized SARS-CoV-2 spike (*S*) gene (Sino Biological, Wayne, PA) encoding the S glycoprotein lacking 18 amino acids at the carboxyl terminus was cloned into the pcDNA3.1 vector. The SARS-CoV-2 spike variants were made by introducing additional mutations into the wild-type (D614) *S* gene using a site-directed mutagenesis kit (Agilent, Santa Clara, CA). The expression plasmid for dimeric soluble ACE2 high-affinity variant 2.4 (sACE2.v2.4) fused to human Fc (Chan et al., 2020) was purchased from Addgene (Watertown, MA (Cat# 154106)). The pcDNA3.1(–)-sACE2 plasmid expressing soluble human ACE2 (1-740aa) with a StrepTag (GGG WSHPQFEK) at the C terminus (sACE2) was made from the pcDNA3.1(–)-ACE2-Strep plasmid (Addgene, catalog no. 1786), by Q5 site-directed mutagenesis (New England Biolabs, Ipswich, MA) (Nguyen et al., 2020). The sACE2-Fc mammalian expression construct is similar to the sACE2 construct but the StrepTag was replaced with the immunoglobulin Fc.

Expression and purification of protein reagents

To produce sACE2.v2.4, sACE2-Fc and sACE2, each expression vector was transfected into Expi293 cells using FectPRO DNA transfection reagent (PolyPlus-transfection). Five days following transfection, sACE2.v2.4 and ACE2-Fc were purified from cell supernatants using Protein A-agarose (Thermo Fisher Scientific) or, in the case of sACE2, Strep-Tactin resin (IBA Lifesciences, Goettingen, Germany), according to the manufacturer's protocol. The soluble SARS-CoV-2 S2P trimer proteins of the D614G, B.1.1.7, B.1.351, P.1 and B.1.1.248 strains were generated by transfecting Expi293 cells with the trimer protein-expressing constructs using FectPRO DNA transfection reagent and purified from cell supernatants 5 days later using

Strep-Tactin resin, according to the manufacturer's protocol (Liu et al., 2020). Two micrograms of each S2P trimer was analyzed on a NuPAGE Bis-Tris protein gel (Invitrogen, Waltham, MA) run at 200 V using MES buffer, after which the gel was stained with Coomassie Blue dye.

VSV pseudotyped by SARS-CoV-2 S glycoproteins

To generate VSV-based vectors pseudotyped with SARS-CoV-2 S glycoproteins, 5×10^6 HEK293T cells were plated in a 10-cm dish one day before transfection. Six micrograms of the SARS-CoV-2 S glycoprotein plasmid was transfected into the HEK293T cells using Polyethylenimine (Polysciences, Warrington, PA). Twenty-four hours later, the cells were infected at a multiplicity of infection of 3 to 5 with rVSV-ΔG pseudovirus bearing a luciferase gene (Kerafast, Boston, MA) for 2 h at 37°C and then washed three times with PBS. Cell supernatants containing pseudoviruses were harvested after another 24 h and clarified by low-speed centrifugation (2000 rpm for 10 min). Viruses were then aliquoted and stored at -80°C until use (Liu et al., 2020; Wang et al., 2021a, 2021b).

Lentiviruses pseudotyped by SARS-CoV-2 S glycoproteins

To generate HIV-based vectors pseudotyped with SARS-CoV-2 S glycoproteins, 5×10^6 HEK293T cells were plated in a 10-cm dish one day before transfection. Then, 6 μg SARS-CoV-2 S glycoprotein expressor plasmid and 6 μg pHIV-1$_{NL4-3}$ ΔEnv-NanoLuc reporter construct were transfected into the HEK293T cells using Polyethylenimine (Polysciences). Cell supernatants containing pseudoviruses were harvested 48 h after transfection and clarified by low-speed centrifugation (2000 rpm for 10 min). Viruses were then aliquoted and stored at -80°C until use.

S glycoprotein expression, processing, and incorporation into pseudovirus particles

HEK293T cells were transfected to produce VSV- and HIV-based particles pseudotyped with SARS-CoV-2 S glycoprotein variants, as described above. To prepare viral particles, cell supernatants were collected, centrifuged at low speed (2000 rpm) to remove cell debris, and pelleted at 18,000 x g for 1 h at 4°C. In parallel with harvesting the pseudoviruses from the cell supernatants, cells were washed and lysed using 1.5% Cymal-5 at 4°C for 10 min. Cell lysates were then clarified by high-speed centrifugation (18,000 x g for 10 min). Cell lysates and virions were analyzed by Western blotting with the following primary antibodies: rabbit anti-SARS-Spike S1 (Sino Biological, Cat# 40591-T62), rabbit anti-SARS-Spike S2 (Sino Biological, Cat# 40590-T62), rabbit anti-p55/p24/p17 (Abcam, Cambridge, MA (Cat# ab63917)), mouse anti-VSV NP (Millipore, Burlington, MA (Cat# MABF2348)) or mouse anti-GAPDH (Millipore, Cat# CB1001). The Western blots were developed with the following secondary antibodies: HRP-conjugated anti-rabbit antibody (Cytiva, Marlborough, MA (NA934-1ML)) or HRP-conjugated goat anti-mouse antibody (Jackson ImmunoResearch, West Grove, PA (Cat# 115-035-008)).

S, S1, and S2 band intensities from unsaturated Western blots were calculated using ImageJ Software. S1/S2 ratios represent the ratios of the intensities of the S1 and S2 glycoprotein bands in the Western blots. The values for the processing index of mutant S glycoproteins were calculated as follows: Processing index = (S1/S × S2/S)$_{mutant}$ ÷ (S1/S × S2/S)$_{WT}$.

Deglycosylation of S glycoproteins

SARS-CoV-2 S glycoproteins in cell lysates or on pseudovirus particles were prepared as described above. Protein samples were boiled in 1 × denaturing buffer and incubated with PNGase F or Endo Hf (New England Biolabs, Ipswich, MA) for 1 h at 37°C according to the manufacturer's protocol. The samples were then analyzed by SDS-PAGE and Western blotting as described above.

Authentic SARS-CoV-2 viruses were obtained from BEI Resources (NIAID, NIH) and propagated for one passage on Vero-E6 cells. To prepare viral particles, cell supernatants were collected, centrifuged at low speed (2000 rpm, 10 min) to remove cell debris, and pelleted at 18,000 x g for 1 h at 4°C. Viral particles then were treated with 1% Triton X-100 and incubated with PNGase F or Endo Hf (New England Biolabs, Ipswich, MA) for 1 h at 37°C according to the manufacturer's protocol. Virions were analyzed by Western blotting with the following primary antibodies: rabbit anti-SARS-Spike S1 (Sino Biological, Cat# 40591-T62), rabbit anti-SARS-Spike S2 (Sino Biological, Cat# 40590-T62), and SARS-CoV-2 Nucleocapsid Protein Monoclonal Antibody (CliniSciences, Cat# bsm-41414M). The Western blots were developed with the following secondary antibodies: HRP-conjugated anti-rabbit antibody (Cytiva, Marlborough, MA

(NA934-1ML)) or HRP-conjugated goat anti-mouse antibody (Jackson ImmunoResearch, West Grove, PA (Cat# 115-035-008)).

Virus infectivity and stability at different temperatures

The pseudoviruses were freshly prepared as described above, without freezing and thawing. The pseudovirus preparations were incubated with target cells seeded in 96-well plates at a density of 3×10^4 cells/well. The target cells were processed as described below.

For VSV-based pseudoviruses, the target cells were cultured for 16-24 hours after infection and then harvested to measure the luciferase activity (Promega, Madison, WI (Cat# E4550)). For HIV-based pseudoviruses, the target cells were cultured for 2-3 days after infection and then cells were harvested to measure the NanoLuc luciferase activity (Promega, Cat# N1120). For authentic SARS-CoV-2 variants, the virus infectious titers were determined by end-point dilution, monitoring cytopathic effects (CPE) on Vero-E6 target cells.

To measure viral stability at different temperatures, pseudoviruses were incubated on ice, at 4°C, at room temperature and at 37°C for different lengths of time prior to measuring their infectivity. Authentic SARS-CoV-2 variants were incubated at 4°C for different lengths of time prior to measuring their infectivity, as described above.

To measure the infectivity of pseudovirus variants on target cells expressing different levels of human ACE2, several dilutions from 1 μg to 0.001 μg of human ACE2 expressor plasmid (Addgene, Watertown, MA (Cat# 1786)) were transfected into 293T cells in 12-well plates using 1 mg/ml PEI. Two days after transfection, cells were trypsinized and used as target cells for measuring the infectivity of VSV pseudotypes. In parallel, ACE2 expression in the transfected cells was measured by FACS and Western blotting, as described below.

For the FACS analysis of ACE2 expression, cells were incubated with a goat anti-ACE2 primary antibody (R&D Systems, Minneapolis, MN (Cat# AF933)), followed by an Alexa 488-conjugated donkey anti-goat secondary antibody (Invitrogen, Cat# A32814). Cells were washed 3 times with FACS buffer (2% FBS in PBS) before each antibody incubation step. Finally, cells were resuspended and ACE2 expression on the cell surface was quantified on a BD FACSCanto™ flow cytometer.

For the Western blot analysis of ACE2 expression, cells were washed and lysed in PBS containing 1.5% Cymal-5 for 10 min. Cell lysates were then clarified by high-speed centrifugation (18,000 x g for 10 min) before being analyzed by Western blotting with a goat anti-ACE2 primary antibody (R&D Systems, Cat# AF933) and an HRP-conjugated mouse anti-goat secondary antibody (Invitrogen, Cat#31400).

Cell-cell fusion assays

For the alpha-complementation assay measuring cell-cell fusion (Figure 3A, left panel), COS-1 effector cells were plated in black-and-white 96-well plates and then cotransfected with a plasmid expressing alpha-gal and either pcDNA3.1 or the SARS-CoV-1 S glycoprotein variant at a 1:1 ratio, using Effectene according to the manufacturer's protocol. At the same time, 293T target cells in 6-well plates were cotransfected with plasmids expressing omega-gal and ACE2 at a 1:1 ratio, using Effectene. Forty-eight hours after transfection, target cells were scraped and resuspended in medium. Medium was removed from the effector cells, and target cells were then added to effector cells (one target-cell well provides sufficient cells for 50 effector-cell wells). Plates were spun at 500 x g for 3 min and then incubated at 37°C in 5% CO2 for 10 h. Medium was aspirated and cells were lysed in Tropix lysis buffer (Thermo Fisher Scientific). The β-galactosidase activity in the cell lysates was measured using the Galacto-Star Reaction Buffer Diluent with Galacto-Star Substrate (Thermo Fisher Scientific), following the manufacturer's protocol.

For the alpha-complementation assay shown in Figure S1, 293T target cells in 6-well plates were cotransfected with serially diluted ACE2 plasmid and 0.2 μg plasmid expressing omega-gal using Effectene.

For the cell-cell fusion assay shown in Figure 3A, right panel, 293T effector cells in 6-well plates were cotransfected with plasmids expressing HIV-1 Tat and ACE2 at a 1:1 ratio, using PEI. Twenty-four hours after transfection, 293T effector cells and TZM-bl cells stably expressing human ACE2 were trypsinized and

cocultured at a ratio of 2:1 in black-and-white 96-well plates in quadruplicate. The cocultured cells were incubated at 37°C in 5% CO_2 for an additional 48 h before luciferase activity was measured.

Spike trimer ELISA

Fifty nanograms of S2P trimer was coated on each well of an ELISA plate at 4°C overnight. Then the plates were blocked with 300 μL of blocking buffer (1% BSA and 10% bovine calf serum in PBS) at 37°C for 2 h. Afterwards, serially diluted sACE2-Fc, convalescent serum, or moderna vaccinee serum was added and incubated at 37°C for 1 h. Next, 100 μL per well of 10,000-fold diluted Peroxidase AffiniPure goat anti-human IgG (H+L) antibody (Jackson ImmunoResearch) was added and incubated for 1 h at 37°C. Between each step, the plates were washed with PBST three times. Finally, the TMB substrate (Sigma, St. Louis, MO) was added and incubated for 5 min at room temperature before the reaction was stopped using 1 M sulfuric acid. Absorbance was measured at 450 nm.

S1 shedding from spike trimers

VSV particles pseudotyped with S glycoprotein variants were prepared as described above. To evaluate spontaneous S1 shedding at different temperatures, the cell supernatants containing pseudoviruses were incubated on ice and at 4°C, room temperature and 37°C for 48 h. Authentic SARS-CoV-2 variants were incubated at 4°C for 1 day and 2 days. Virus particles were then pelleted at 18,000 x g for 1 h at 4°C. The pelleted samples were resuspended in 1 X LDS sample buffer (Invitrogen, Cat# NP0008) and analyzed by Western blotting. To evaluate soluble ACE2-induced S1 shedding, the cell supernatants containing pseudovirus particles were incubated with soluble ACE2 at different concentrations on ice for 1 h. Afterwards, virus particles were pelleted at 18,000 x g for 1 h at 4°C. The pelleted virus particles were washed twice with cold PBS before the samples were resuspended in 1 X LDS sample buffer and analyzed by Western blotting. S1, S2 and NP were detected as described above; soluble ACE2 bound to the pseudovirus particles was detected with a goat anti-ACE2 primary antibody (R&D Systems, Cat# AF933) and an HRP-conjugated rabbit anti-goat secondary antibody (Invitrogen, Cat#31400).

Neutralization assay

We evaluated the neutralization of pseudoviruses by sACE2.v2.4, six sera collected from March to June 2020 from New York City patients that recovered from COVID-19 and six sera from Moderna vaccinees (Wang et al., 2021b). Pseudovirus neutralization assays were performed by incubating VSV vectors pseudotyped by S glycoprotein variants with serial dilutions of sACE2.v2.4, sera from convalescent COVID-19 patients or vaccinee sera in triplicate in 96-well plates for 1 h at 37°C. Approximately 3×10^4 target cells (Vero-E6 or 293T-ACE2 cells) per well were then added. The cultures were maintained for an additional 16-24 h at 37°C before luciferase activity was measured as described above. Neutralization activity was calculated from the reduction in luciferase activity compared with mock-treated controls.

For the authentic SARS-CoV-2 neutralization assay, serially diluted serum samples starting from 1:100 were incubated with the SARS-CoV-2 preparation for 1 hour at 37°C in triplicate. Then, the virus-serum mixture was transferred to Vero-E6 cells that had been grown overnight in 96-well plates. The multiplicity of infection of the uninhibited virus preparation was 0.1. The cells were incubated for 3 days before the cytopathic effects of viral infection were visually scored for each well in a blinded fashion by two independent observers. The results were then converted into percentage neutralization at a given serum dilution.

The concentrations of sACE2.v2.4 and serum titers that inhibit 50% of infection (the IC_{50} and ID_{50} values, respectively) were determined by fitting the data in five-parameter dose-response curves in GraphPad Prism 8 (GraphPad Software Inc., San Diego, CA).

QUANTIFICATION AND STATISTICAL ANALYSIS

Evaluations of statistical significance were performed employing Student's unpaired or paired *t* test using GraphPad Prism 8 software. Levels of significance are indicated as follows: $*p<0.05$; $**p<0.01$; $***p<0.001$; and $****p<0.0001$. EC_{50}, IC_{50} and ID_{50} values were determined by fitting the data in five-parameter dose-response curves in GraphPad Prism 8. Western blot data were analyzed by Image Lab and ImageJ software. FACS analysis was performed by a BD FACSCanto™ flow cytometer and data was analyzed using FlowJo 10 software. All data presented in this manuscript are representative of mean values derived from at least two independent experiments.